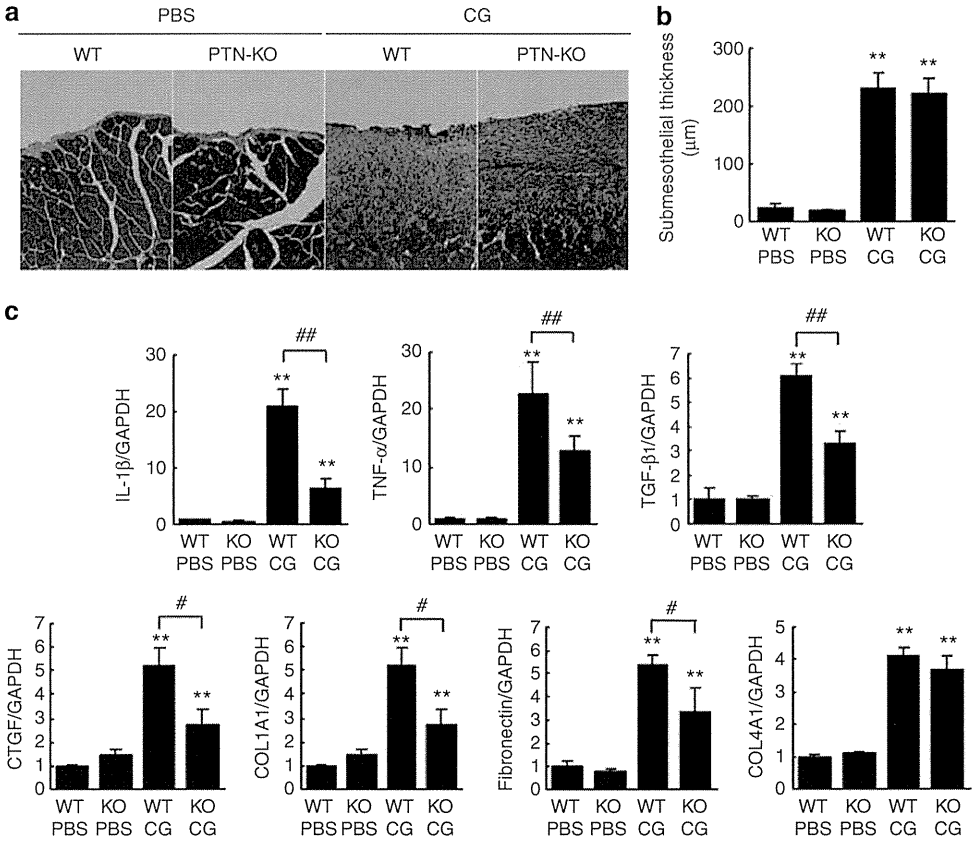

Figure 4 | Histological appearance and mRNA expression of peritoneum in PTN knockout mice (C57BL/6J background).[13] Pleiotrophin (PTN) knockout mice were treated with chlorhexidine gluconate (CG) three times a week for 4 weeks. (**a**) Masson's trichrome staining of peritoneum in wild-type or PTN knockout mice treated with phosphate-buffered saline (PBS) or CG. (**b**) The thickness of peritoneal membrane in mice. (**c**) Real-time reverse transcriptase-polymerase chain reaction analyses of interleukin (IL)-1β, tumor necrosis factor (TNF)-α, transforming growth factor (TGF)-β1, connective tissue growth factor (CTGF), fibronectin, α1(I) collagen (COL1A1), and a1(IV) collagen (COL4A1). GAPDH was used as control. WT PBS: $n=5$, KO PBS: $n=4$, WT CG: $n=11$, KO CG: $n=10$. Mean ± s.e. $^{**}P<0.01$ vs. PBS-treated mice with the same genotype. $^{\#}P<0.05$, $^{\#\#}P<0.01$. GAPDH, glyceraldehyde-3-phosphate dehydrogenase; KO, PTN knockout mice; WT, wild-type mice.

fibrin degradation products also correlate with increased peritoneal permeability.[22] IL-6 is an acute-phase inflammatory reaction protein. The dialysate and ascite levels of inflammatory and fibrinolysis markers have been reported to increase before the development of encapsulating peritoneal sclerosis.[23] Although levels of inflammatory, angiogenic, and fibrinolytic markers such as IL-6, vascular endothelial growth factor, and fibrin degradation products could be important biomarkers for developing encapsulating peritoneal sclerosis, key molecules involved in the process of peritoneal damage are still elusive. In this study, we performed microarray analysis to identify genes differentially expressed between PBS-treated and CG-treated mice and expressed in cultured mesothelial cells. *Procollagen type VIII α1* gene and IL-6 were upregulated by 73.5- and 25.9-fold, respectively. These genes have been already reported under peritoneal damage, indicating that our microarray analysis is consistent with previous reports.[4,24] Genes identified by microarray analysis can be candidate ones for elucidating the development and progression of peritoneal fibrosis. In this study, we detected increased PTN mRNA expression and protein levels by 42- and 4-fold, respectively. The discrepancy between mRNA and protein levels may come from long half-life of the protein.[25] Our study revealed that human peritoneal biopsy samples contained PTN mRNA and protein. PTN protein in human peritoneum was located at mesothelial cells and fibroblasts, consistent with mouse peritoneal fibrosis model. We also revealed that PTN was detected in overnight-dwell peritoneal dialysate and that the main form of PTN in peritoneal dialysate is 15 kDa. Previously, Lu *et al.*[14] have demonstrated that PTN15 promotes glioblastoma proliferation in an ALK-dependent manner, whereas PTN18 promotes migration in a Ptprz1-dependent manner. Peritoneal dialysates from patients with peritonitis may contain high levels of PTN.

PTN mRNA expression was increased in peritoneal fibrosis model mice mainly at fibroblasts. *In vitro* study also showed that PTN expression was abundant in cultured fibroblasts compared with cultured mesothelial cells, lymphocytes, and macrophages. PTN gene expression has been shown to be upregulated in NIH3T3 fibroblasts stimulated by

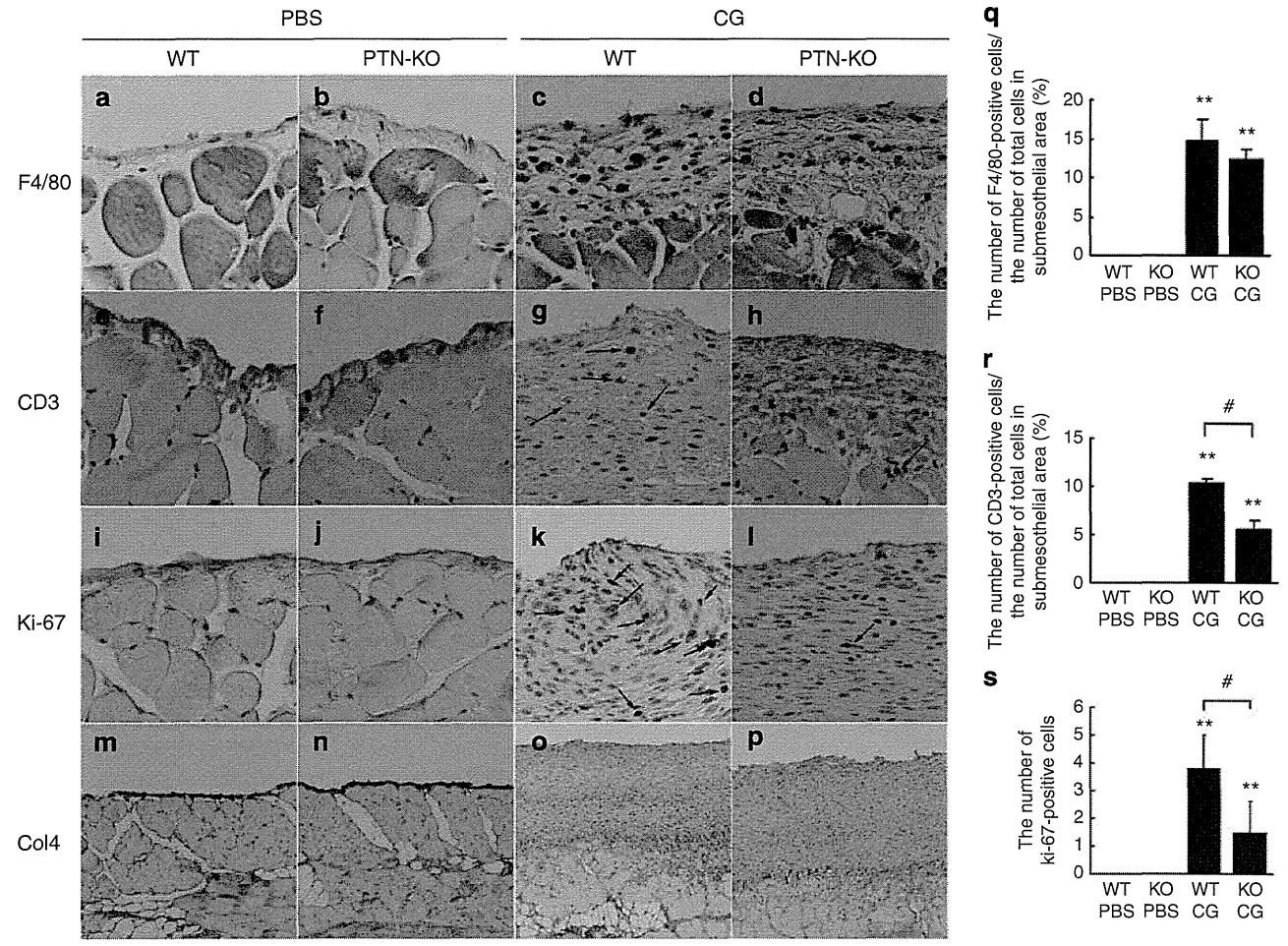

Figure 5 | Immunohistochemical study of F4/80, CD3, Ki-67, and type IV collagen (Col4). Mice were treated with chlorhexidine gluconate (CG) three times a week for 4 weeks. (**a**–**d**) F4/80, (**e**–**h**) CD3, (**i**–**l**) Ki67, and (**m**–**p**) Col4 staining in the peritoneum from (**a**, **e**, **i**, and **m**) phosphate-buffered saline (PBS)-injected wild-type (WT) mice, (**b**, **f**, **j**, and **n**) PBS-injected PTN knockout (KO) mice, (**c**, **g**, **k**, and **o**) CG-injected WT mice, (**d**, **h**, **l**, and **p**) CG-injected pleiotrophin (PTN)-KO mice. Arrows indicate positive cells. (**q**) The number of F4/80-positive cells per the number of total cells in the submesothelial area in mice. (**r**) The number of CD3-positive cells per the number of total cells in the submesothelial area in mice. (**s**) The number of Ki67-positive proliferated cells in the submesothelial area in mice. WT PBS: $n = 5$, KO PBS: $n = 4$, WT CG: $n = 11$, KO CG: $n = 10$. Mean ± s.e. $^{**}P < 0.01$ vs. PBS-treated mice with the same genotype in Figure 5. $^{\#}P < 0.05$.

platelet-derived growth factor-AB.[26] A recent paper reveals that PTN expression is strongly associated with IFN-γ/JAK/STAT1 signaling.[27] Further investigations are necessary to elucidate the molecular mechanism of PTN induction. PTN is a ligand of the RPTPβ/ζ,[12,28] ALK[12,] and syncecan-3.[12] Our study showed that RPTPβ/ζ was expressed in mesothelial cells, not in cultured fibroblasts, lymphocytes, or macrophages, and that syndecan-3 highly existed in mesothelial cells and was weakly expressed in fibroblasts and macrophages. ALK[29] was not detected in these cells. Taken together, PTN secreted by fibroblasts in submesothelial layer can have an effect on proliferation and migration mainly in mesothelial cells that express RPTPβ/ζ and syndecan-3.[30] The role of PTN receptors in peritoneal fibrosis needs further clarification.

In this study, the role of PTN in peritoneal fibrosis was investigated by using PTN-deficient mice. Without PTN, inflammatory and profibrotic responses were significantly reduced at 4 weeks after CG treatment, suggesting that PTN aggravates inflammation and fibrosis in the development of peritoneal fibrosis. Increased peritoneal permeability, examined by peritoneal equilibration tests, in CG-treated wild-type mice was almost completely ameliorated in CG-treated PTN knockout mice, suggesting that PTN can increase peritoneal permeability. Although CG-injected PTN knockout mice showed lower expression of COL1A1 and fibronectin than wild-type mice, the thickness of peritoneal membranes did not change between PTN-deficient mice and wild-type mice. The reason may come from similar expression levels of some other types of extracellular matrix such as collagen IV. Type IV collagen is abundantly deposited in peritoneal membrane.[31,32] Although macrophage infiltration has been shown to be an important phenomenon in peritoneal fibrosis,[33] CG-treated PTN-deficient mice showed no apparent difference in macrophage infiltration compared with wild-type mice. T cells are also an important part of

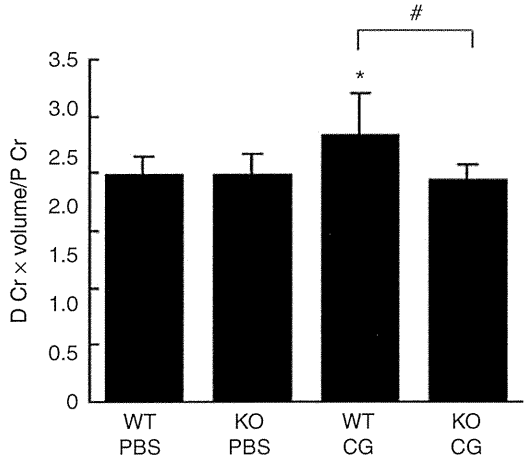

Figure 6 | Modified peritoneal equilibration test (PET). D Cr × volume/P Cr represents the creatinine (Cr) level of 7% glucose dialysate effluent (D) multiplied by volume divided by that of plasma (P) level in mice at 2 h retention. Chlorhexidine gluconate (CG)-injected wild-type (WT) mice showed increased D Cr × volume/P Cr compared with phosphate-buffered saline (PBS)-injected mice. Pleiotrophin (PTN)-knockout (KO) mice treated with CG showed reduced D Cr × volume/P Cr level compared with WT mice with CG. WT PBS: $n=3$, KO PBS: $n=6$, WT CG: $n=5$, KO CG: $n=7$. Mean ± s.e. $^{*}P<0.05$ vs. PBS-treated mice with the same genotype in Figure 6. $^{\#}P<0.05$.

peritoneal membrane damage,[34,35] and our results showed that T-cell infiltration was reduced in CG-treated PTN-deficient mice. PTN has been shown to induce expression of inflammatory cytokines in peripheral blood mononuclear cells.[36] The mechanism of T-cell infiltration by PTN is not clear, because RPTPβ/ζ mRNA nor syndecan-3 are not detected in cultured T-cell line. Downstream mediators of PTN need to be investigated in the future study. Cell proliferation was assessed by Ki-67 immunostaining.[37] PTN-deficient mice showed lower expression of Ki-67, indicating that cell proliferation in submesothelial layer was inhibited without PTN.

In conclusion, this study shows that PTN expression is upregulated in a mouse model of peritoneal fibrosis and is present in human peritoneal tissues and in peritoneal dialysate effluent, and that PTN secreted by fibroblasts or mesothelial cells can have a proliferative and chemotactic effect on mesothelial cells, and that PTN-deficient mice exhibit a weaker peritoneal membrane damage. These findings can be a help to elucidate a novel pathway in peritoneal fibrosis and suggest that PTN could be a promising biomarker against peritoneal damage.

MATERIALS AND METHODS

Patients

Patients who were admitted to Kyoto University Hospital for the diagnosis and treatment of renal disorders were enrolled under informed consent. This study was approved by the ethics committee on human research of Kyoto University Graduate School of Medicine. The parietal peritoneal samples were taken from the insertion site of a PD catheter located in the lumbar region as biopsies at the beginning or ending of PD. Peritoneal dialysate effluents were obtained at the time of the exchange. Expression of PTN in peritoneal biopsy sample was assessed by the RT-PCR method. After RNA extraction by RNeasy mini kit (Qiagen, Valencia, CA), complementary DNA was generated using the SuperScript II Reverse Transcriptase (Invitrogen, Carlsbad, CA) according to the manufacturer's instruction. RT-PCR was performed using the following primers: forward, 5′-gggaagaaagagaccagtgagt-3′ and reverse, 5′-ctggtttctctttcttccctgc-3′.

Induction of peritoneal fibrosis and phenotypic analysis

All animal experiments were approved by the animal experimentation committee of Kyoto University Graduate School of Medicine. Peritoneal fibrosis was induced in mice with the intraperitoneal injections of 0.3 ml of 0.1% CG in 15% ethanol and 85% PBS three times a week for 1, 2, 3, and 4 weeks as previously reported ($n=5$, each).[38] For evaluating dose–response, mice were administered 0.3 ml of 0.01% and 0.03% CG in 15% ethanol and 85% PBS three times a week for 4 weeks. Control mice received intraperitoneal injection of PBS. Mice were killed under pentobarbital anesthesia, and peritoneal tissues were obtained from the upper portion of the parietal peritoneum to avoid injured peritoneum by repeated injections.

For dialysis fluid infusion, silicone port catheters with two cuffs were used (PennyPort MMP-4S; Access Technologies, Skokie, IL). After mice were anesthetized under pentobarbital, an incision was made in the skin of the back and left lumbar portion. Peritoneal membrane was pricked with a 20-Gy needle to make a small hole. The catheter port was implanted under the skin of the back and the catheters were inserted along the needle hole. A catheter port was placed subcutaneously on the back. One milliliter of PDFs (Perisate; JMS, Hiroshima, Japan) containing 7% PD solution or PBS were administered intraperitoneally via a catheter port using a 26-Gy needle every day for 4 weeks ($n=5$, each). PTN-deficient mice (C57BL/6J background) were generated as described previously.[13]

Modified peritoneal equilibration test

Modified peritoneal equilibration test was conducted to determine the peritoneal permeability. Wild-type or PTN knockout mice were injected with PBS or CG ($n=5$, each) three times for 2 weeks, and were then administered intraperitoneal injection of 3 ml of 7% glucose dialysis solution (Perisate; JMS). After 2 h of retention, dialysis fluids were collected and blood samples were withdrawn. Serum and dialysate creatinine levels were measured by using the enzymatic method (SRL, Tokyo, Japan).

Affymetrix gene chip array

Wild-type mice were subjected to peritoneal fibrosis with the intraperitoneal injections of 0.3 ml of 0.1% CG in 15% ethanol and 85% PBS three times a week for 3 weeks ($n=3$). As control, PBS-treated wild-type mice were used ($n=3$). Total RNA from the parietal peritoneum at day 21 was extracted by RNeasy Mini Kit (Qiagen) in these mice.[39] Complementary RNA probes were generated using the GeneChip Expression 3′-Amplification Reagents for IVT Labeling Kit (Applied Biosystems, Foster city, CA) and each sample was hybridized to an Affymetrix mouse genome 430 2.0 array at TAKARA Bio (Shiga, Japan). After washing, the genechips were scanned by a GeneChip Scanner 3000. Data normalization, log transformation, statistical analysis, and pattern study were performed with the GeneChip Operating Software.

Histology and immunohistochemistry

Peritoneal membrane sections were fixed with 4% buffered paraformaldehyde and embedded in paraffin. Sections (1 μm thick) were stained with Masson's trichrome.[40] We measured the thickness of the fibrotic submesothelial zone above the abdominal muscle layer in cross-sections as described previously,[41] by using MetaMorph software (Molecular Devices, Downingtown, PA). Ten different points were examined by two investigators without knowledge of the origin of the slides. The results were expressed as the average peritoneal membrane thickness. For immunohistochemical analyses of PTN, collagen type IV, F4/80, CD3, and Ki-67 in mice, the sections were processed as described.[40] After antigen retrieval, the samples were incubated with rabbit polyclonal anti-PTN antibody (ProteinTech Group, Chicago, IL), rabbit polyclonal anti-mouse collagen type IV antibody (Millipore, Billerica, MA), rat monoclonal anti-F4/80 antibody (Serotec, Oxford, UK), rabbit polyclonal anti-CD3 antibody (DAKO, Glostrup, Denmark), and rat monoclonal anti-Ki-67 antibody (DAKO). After incubation with horseradish peroxidase-conjugated secondary antibodies, the specimens were developed using 3,3′-diaminobenzidine tetrahydrochloride. For immunohistochemical study of human PTN, we used a rabbit polyclonal anti-PTN antibody (Abcam, Cambridge, UK) as a primary antibody.

Real-time PCR analysis

Quantitative real-time PCR was performed using Premix Ex Taq (TAKARA Bio) on an Applied Biosystems 7300 real-time PCR system (Applied Biosystems) or a StepOnePlus system (Applied Biosystems), as described previously with some modification.[39] To determine mouse PTN, Ptprz1, TGF-β1, connective tissue growth factor, COL1A1, COL4A1, fibronectin, and IL-1β and tumor necrosis factor-α expression levels, gene-specific primers and probes were used. Primers and probe sequences are listed in Supplementary Table S1 online. Expression of each mRNA was normalized for glyceraldehyde-3-phosphate dehydrogenase using TaqMan Rodent glyceraldehyde-3-phosphate dehydrogenase control reagents (Applied Biosystems).

Western blot analysis

Western blot analysis was performed as described.[39] Filters transferred onto protein extracts or peritoneal dialysate effluents were incubated with rabbit polyclonal anti-PTN antibody (ProteinTech Group) and mouse monoclonal anti-glyceraldehyde-3-phosphate dehydrogenase antibody (Santa Cruz Biotechnology, Santa Cruz, CA). Immunoblots were then developed using a chemiluminescence kit (GE healthcare, Piscataway, NJ).

Cell culture

Mouse peritoneal mesothelial cells were obtained using a standard trypsin/ethylenediaminetetraacetic acid digestion method from the peritoneal wall of adult male C57BL/6J mice.[42,43] The excised peritoneal flap was cut into small pieces and then incubated, with constant agitation, with 0.25% trypsin and 1 mmol/l ethylenediaminetetraacetic acid (Invitrogen) for 15 min at 37 °C. The released cells were centrifuged at 1200 r.p.m. for 5 min and cultured with Dulbecco's Modified Eagle Medium (DMEM D6046; Sigma-Aldrich, St Louis, MI) supplemented with 10% fetal bovine serum (FBS), penicillin (100 U/ml), streptomycin (100 μg/ml), and amphotericin B (25 ng/ml). NIH3T3 fibroblasts, RAW264.7 cells, and bEnd.3 cells were obtained from American Type Culture Collection (Manassas, VA). BW5147 cells were provided by Health Science Research Bank (Sennan, Osaka, Japan) and BCL1-B20 cells were provided by the RIKEN BRC through the National Bio-Resource Project of the Ministry of Education, Culture, Sports, Science and Technology, Japan. BCL1-B20 cells were cultured with RPMI1640 (Sigma) with 10% FBS. Other cells were cultured with DMEM with 10% FBS.

Proliferation assay in cultured mesothelial cells was performed with ^{3}H-thymidine as described previously.[44] Briefly, mesothelial cells were plated on 24-well plates ($n = 6$, each group) and incubated with DMEM containing 0.3% FBS for the 24 h. Cell proliferation was studied in the presence of 1 ng/ml of recombinant human PTN (R&D Systems, Minneapolis, MN), 10 ng/ml of recombinant human platelet-derived growth factor-BB (BD Biosciences, San Jose, CA), 10^{-6} mol/l of angiotensin II (Peptide Institute, Osaka, Japan), 100 ng/ml of recombinant human endothelial growth factor (PeproTech EC, London, UK), or vehicle (PBS) for 24 h with DMEM containing 0.3% FBS. ^{3}H-thymidine was added simultaneously with the above-described agents. Migration assay was performed as described previously.[45] In brief, migration of mesothelial cells was analyzed by modified Boyden chamber method using 96-well chemotaxis chambers. In the upper chambers, mesothelial cells were placed with DMEM containing 0.02% bovine serum albumin. In the lower chambers, there were serum-free DMEM containing PTN (1 ng/ml), platelet-derived growth factor-BB (50 ng/ml), angiotensin II (10^{-6} mol/l), or endothelial growth factor (100 ng/ml). The cells were incubated for 4 h and the filters were stained with 0.5% Coomassie Brilliant Blue R250 (Nacalai Tesque, Kyoto, Japan) in 50% methanol, 40% water, and 10% acetic acid ($n = 6$, each).

Statistical analysis

Data are expressed as the mean ± s.e. Statistical analysis was performed using one-way analysis of variance as appropriate. A P-value < 0.05 was considered statistically significant.

DISCLOSURE

All the authors declared no competing interests.

ACKNOWLEDGMENTS

We gratefully acknowledge M Fujimoto and Y Sakashita and other lab members for technical assistance, and A Yamamoto for secretarial assistance. This work was supported in part by research grants from the Japanese Ministry of Education, Culture, Sports, Science and Technology, the Japanese Ministry of Health, Labour and Welfare, and Japan Baxter PD Fund.

SUPPLEMENTARY MATERIAL

Table S1. TaqMan primers and probe sequences.

Supplementary material is linked to the online version of the paper at http://www.nature.com/ki

REFERENCES

1. Ledebo I, Ronco C. The best dialysis therapy? Results from an international survey among nephrology professionals. *NDT Plus* 2008; **1**: 403–408.
2. Saxena R. Pathogenesis and treatment of peritoneal membrane failure. *Pediatr Nephrol* 2008; **23**: 695–703.
3. Yung S, Chan TM. Preventing peritoneal fibrosis—insights from the laboratory. *Perit Dial Int* 2003; **23**(S2): S37–S41.
4. Pecoits-Filho R, Araujo MR, Lindholm B *et al.* Plasma and dialysate IL-6 and VEGF concentrations are associated with high peritoneal solute transport rate. *Nephrol Dial Transplant* 2002; **17**: 1480–1486.
5. Lai KN, Lai KB, Szeto CC *et al.* Growth factors in continuous ambulatory peritoneal dialysis effluent. Their relation with peritoneal transport of small solutes. *Am J Nephrol* 1999; **19**: 416–422.

6. Oh KH, Jung JY, Yoon MO *et al.* Intra-peritoneal interleukin-6 system is a potent determinant of the baseline peritoneal solute transport in incident peritoneal dialysis patients. *Nephrol Dial Transplant* 2010; **25**: 1639–1646.
7. Margetts PJ, Kolb M, Galt T *et al.* Gene transfer of transforming growth factor-β1 to the rat peritoneum: effects on membrane function. *J Am Soc Nephrol* 2001; **12**: 2029–2039.
8. Margetts PJ, Kolb M, Yu L *et al.* Inflammatory cytokines, angiogenesis, and fibrosis in the rat peritoneum. *Am J Pathol* 2002; **160**: 2285–2294.
9. Aroeira LS, Aguilera A, Selgas R *et al.* Mesenchymal conversion of mesothelial cells as a mechanism responsible for high solute transport rate in peritoneal dialysis: role of vascular endothelial growth factor. *Am J Kidney Dis* 2005; **46**: 938–948.
10. Zakaria el R, Matheson PJ, Hurt RT *et al.* Chronic infusion of sterile peritoneal dialysis solution abrogates enhanced peritoneal gene expression responses to chronic peritoneal catheter presence. *Adv Perit Dial* 2008; **24**: 7–15.
11. Deuel TF, Zhang N, Yeh HJ *et al.* Pleiotrophin: a cytokine with diverse functions and a novel signaling pathway. *Arch Biochem Biophys* 2002; **397**: 162–171.
12. Jin L, Jianghai C, Juan L *et al.* Pleiotrophin and peripheral nerve injury. *Neurosurg Rev* 2009; **32**: 387–393.
13. Muramatsu H, Zou P, Kurosawa N *et al.* Female infertility in mice deficient in midkine and pleiotrophin, which form a distinct family of growth factors. *Genes Cells* 2006; **11**: 1405–1417.
14. Lu KV, Jong KA, Kim GY *et al.* Differential induction of glioblastoma migration and growth by two forms of pleiotrophin. *J Biol Chem* 2005; **280**: 26953–26964.
15. Milner PG, Li YS, Hoffman RM *et al.* A novel 17 kD heparin-binding growth factor (HBGF-8) in bovine uterus: purification and N-terminal amino acid sequence. *Biochem Biophys Res Commun* 1989; **165**: 1096–1103.
16. Rauvala H. An 18-kd heparin-binding protein of developing brain that is distinct from fibroblast growth factors. *EMBO J* 1989; **8**: 2933–2941.
17. Sakurai H, Bush KT, Nigam SK. Identification of pleiotrophin as a mesenchymal factor involved in ureteric bud branching morphogenesis. *Development* 2001; **128**: 3283–3293.
18. Amet LE, Lauri SE, Hienola A *et al.* Enhanced hippocampal long-term potentiation in mice lacking heparin-binding growth-associated molecule. *Mol Cell Neurosci* 2001; **17**: 1014–1024.
19. Ochiai K, Muramatsu H, Yamamoto S *et al.* The role of midkine and pleiotrophin in liver regeneration. *Liver Int* 2004; **24**: 484–491.
20. Yamamoto R, Nakayama M, Hasegawa T *et al.* High-transport membrane is a risk factor for encapsulating peritoneal sclerosis developing after long-term continuous ambulatory peritoneal dialysis treatment. *Adv Perit Dial* 2002; **18**: 131–134.
21. Kawanishi H, Moriishi M. Encapsulating peritoneal sclerosis: prevention and treatment. *Perit Dial Int* 2007; **27**(S2): S289–S292.
22. Kawanishi H, Fujimori A, Tsuchida K *et al.* Markers in peritoneal effluent for withdrawal from peritoneal dialysis: multicenter prospective study in Japan. *Adv Perit Dial* 2005; **21**: 134–138.
23. Kawanishi H, Harada Y, Noriyuki T *et al.* Treatment options for encapsulating peritoneal sclerosis based on progressive stage. *Adv Perit Dial* 2001; **17**: 200–204.
24. Xu X, Rivkind A, Pappo O *et al.* Role of mast cells and myofibroblasts in human peritoneal adhesion formation. *Ann Surg* 2002; **236**: 593–601.
25. Dreyfus J, Brunet-de Carvalho N, Duprez D *et al.* HB-GAM/pleiotrophin: localization of mRNA and protein in the chicken developing leg. *Int J Dev Biol* 1998; **42**: 189–198.
26. Li YS, Gurrieri M, Deuel TF. Pleiotrophin gene expression is highly restricted and is regulated by platelet-derived growth factor. *Biochem Biophys Res Commun* 1992; **184**: 427–432.
27. Li F, Tian F, Wang L *et al.* Pleiotrophin (PTN) is expressed in vascularized human atherosclerotic plaques: IFN-γ/JAK/STAT1 signaling is critical for the expression of PTN in macrophages. *FASEB J* 2010; **24**: 810–822.
28. Meng K, Rodriguez-Pena A, Dimitrov T *et al.* Pleiotrophin signals increased tyrosine phosphorylation of β-catenin through inactivation of the intrinsic catalytic activity of the receptor-type protein tyrosine phosphatase β/ζ. *Proc Natl Acad Sci U S A* 2000; **97**: 2603–2608.
29. Stoica GE, Kuo A, Aigner A *et al.* Identification of anaplastic lymphoma kinase as a receptor for the growth factor pleiotrophin. *J Biol Chem* 2001; **276**: 16772–16779.
30. Raulo E, Chernousov MA, Carey DJ *et al.* Isolation of a neuronal cell surface receptor of heparin binding growth-associated molecule (HB-GAM). Identification as N-syndecan (syndecan-3). *J Biol Chem* 1994; **269**: 12999–13004.
31. Mateijsen MA, van der Wal AC, Hendriks PM *et al.* Vascular and interstitial changes in the peritoneum of CAPD patients with peritoneal sclerosis. *Perit Dial Int* 1999; **19**: 517–525.
32. Saito H, Kitamoto M, Kato K *et al.* Tissue factor and factor V involvement in rat peritoneal fibrosis. *Perit Dial Int* 2009; **29**: 340–351.
33. Schilte MN, Celie JW, Wee PM *et al.* Factors contributing to peritoneal tissue remodeling in peritoneal dialysis. *Perit Dial Int* 2009; **29**: 605–617.
34. Glik A, Douvdevani A. T lymphocytes: the 'cellular' arm of acquired immunity in the peritoneum. *Perit Dial Int* 2006; **26**: 438–448.
35. Devuyst O, Margetts PJ, Topley N. The pathophysiology of the peritoneal membrane. *J Am Soc Nephrol* 2010; **21**: 1077–1085.
36. Achour A, M'Bika JB, Baudouin F *et al.* Pleiotrophin induces expression of inflammatory cytokines in peripheral blood mononuclear cells. *Biochimie* 2008; **90**: 1791–1795.
37. Endl E, Gerdes J. The Ki-67 Protein: Fascinating forms and an unknown function. *Exp Cell Res* 2000; **257**: 231–237.
38. Ishii Y, Sawada T, Shimizu A *et al.* An experimental sclerosing encapsulating peritonitis model in mice. *Nephrol Dial Transplant* 2001; **16**: 1262–1266.
39. Yokoi H, Mukoyama M, Mori K *et al.* Overexpression of connective tissue growth factor in podocytes worsens diabetic nephropathy in mice. *Kidney Int* 2008; **73**: 446–455.
40. Yokoi H, Mukoyama M, Nagae T *et al.* Reduction in connective tissue growth factor by antisense treatment ameliorates renal tubulointerstitial fibrosis. *J Am Soc Nephrol* 2004; **15**: 1430–1440.
41. Yoshio Y, Miyazaki M, Abe K *et al.* TNP-470, an angiogenesis inhibitor, suppresses the progression of peritoneal fibrosis in mouse experimental model. *Kidney Int* 2004; **66**: 1677–1685.
42. Tamura M, Osajima A, Nakayamada S *et al.* High glucose levels inhibit focal adhesion kinase-mediated wound healing of rat peritoneal mesothelial cells. *Kidney Int* 2003; **63**: 722–731.
43. Yung S, Li FK, Chan TM. Peritoneal mesothelial cell culture and biology. *Perit Dial Int* 2006; **26**: 162–173.
44. Suganami T, Mukoyama M, Sugawara A *et al.* Overexpression of brain natriuretic peptide in mice ameliorates immune-mediated renal injury. *J Am Soc Nephrol* 2001; **12**: 2652–2663.
45. Sawai K, Mori K, Mukoyama M *et al.* Angiogenic protein Cyr61 is expressed by podocytes in anti-Thy-1 glomerulonephritis. *J Am Soc Nephrol* 2003; **14**: 1154–1163.

Diabetologia (2012) 55:2256–2266
DOI 10.1007/s00125-012-2578-1

ARTICLE

Exacerbation of diabetic nephropathy by hyperlipidaemia is mediated by Toll-like receptor 4 in mice

T. Kuwabara · K. Mori · M. Mukoyama · M. Kasahara · H. Yokoi · Y. Saito · Y. Ogawa · H. Imamaki · T. Kawanishi · A. Ishii · K. Koga · K. P. Mori · Y. Kato · A. Sugawara · K. Nakao

Received: 3 February 2012 / Accepted: 4 April 2012 / Published online: 19 May 2012

Abstract
Aims/hypothesis Hyperlipidaemia is an independent risk factor for the progression of diabetic nephropathy, but its molecular mechanism remains elusive. We investigated in mice how diabetes and hyperlipidaemia cause renal lesions separately and in combination, and the involvement of Toll-like receptor 4 (TLR4) in the process.
Methods Diabetes was induced in wild-type (WT) and *Tlr4* knockout (KO) mice by intraperitoneal injection of streptozotocin (STZ). At 2 weeks after STZ injection, normal diet was substituted with a high-fat diet (HFD). Functional and histological analyses were carried out 6 weeks later.
Results Compared with treatment with STZ or HFD alone, treatment of WT mice with both STZ and HFD markedly aggravated nephropathy, as indicated by an increase in albuminuria, mesangial expansion, infiltration of macrophages and upregulation of pro-inflammatory and extracellular-matrix-associated gene expression in glomeruli. In *Tlr4* KO mice, the addition of an HFD to STZ had almost no effects on the variables measured. Production of protein S100 calcium binding protein A8 (calgranulin A; S100A8), a potent ligand for TLR4, was observed in abundance in macrophages infiltrating STZ-HFD WT glomeruli and in glomeruli of diabetic nephropathy patients. High-glucose and fatty acid treatment synergistically upregulated *S100a8* gene expression in macrophages from WT mice, but not from KO mice. As putative downstream targets of TLR4, phosphorylation of interferon regulatory factor 3 (IRF3) was enhanced in kidneys of WT mice co-treated with STZ and HFD.
Conclusions/interpretation Activation of S100A8/TLR4 signalling was elucidated in an animal model of diabetic glomerular injury accompanied with hyperlipidaemia, which may provide novel therapeutic targets in progressive diabetic nephropathy.

Keywords Diabetic nephropathy · Glomerulus · High-fat diet · Hyperlipidaemia · Macrophages · S100A8 · TLR4

Abbreviations

BMDMs	Bone marrow-derived macrophages
C_t	Cycle threshold
CTGF	Connective tissue growth factor
ECM	Extracellular matrix
ESRD	End-stage renal disease
GAPDH	Glyceraldehyde-3-phosphate dehydrogenase
HFD	High-fat diet
IKB	Inhibitor κB
IRF3	Interferon regulatory factor 3
JNK	c-Jun N-terminal kinase
KO	Knockout
MAC-2	Lectin galactoside-binding, soluble, 3
MYD88	Myeloid differentiation primary response gene (88)
ND	Normal diet
nSTZ	non-STZ
PAS	periodic acid–Schiff

Electronic supplementary material The online version of this article (doi:10.1007/s00125-012-2578-1) contains peer-reviewed but unedited supplementary material, which is available to authorised users.

T. Kuwabara · K. Mori (✉) · M. Mukoyama · M. Kasahara · H. Yokoi · Y. Saito · H. Imamaki · T. Kawanishi · A. Ishii · K. Koga · K. P. Mori · Y. Kato · K. Nakao
Department of Medicine and Clinical Science, Kyoto University Graduate School of Medicine, 54 Shogoin Kawaharacho, Sakyoku, Kyoto 606-8507, Japan
e-mail: keyem@kuhp.kyoto-u.ac.jp

Y. Ogawa · A. Sugawara
Department of Nephrology, Osaka Redcross Hospital, Osaka, Japan

S100A8	S100 calcium binding protein A8
S100A9	S100 calcium binding protein A9
STZ	Streptozotocin
TLR	Toll-like receptor
TRIF	TIR-domain-containing adapter-inducing interferon-β
WT	Wild-type

Introduction

Diabetic nephropathy is one of the most prevalent causes of end-stage renal disease (ESRD) [1]. Despite progress in pharmacological strategies to control diabetes, hypertension and other metabolic abnormalities, the number of patients entering ESRD because of diabetic nephropathy remains extremely high, and the development of new classes of therapeutic reagents is eagerly anticipated [2]. During recent decades, the pathophysiology of diabetic nephropathy has become complex and serious because of coexisting lifestyle-related disorders, such as hyperlipidaemia, hypertension and obesity [3]. In fact, hyperlipidaemia is an independent risk factor for the progression of diabetic nephropathy in both type 1 and type 2 diabetes [4, 5], but the underlying molecular mechanism remains elusive [6].

Toll-like receptors (TLRs) are a family of receptors that play a critical role in the innate immune system by activating pro-inflammatory signalling pathways in response to molecular patterns synthesised by microorganisms [7]. TLR4, one of the best-characterised TLRs, binds with lipopolysaccharide from Gram-negative bacterial cell walls and with several endogenous ligands [7]. TLR4 also plays an important role in various kidney disorders, such as glomerulonephritis, renal ischaemia and diabetic tubular inflammation [8–13], but the role of TLR4 in diabetic glomerular injury and hyperlipidaemia-induced kidney damage remains largely unknown.

In the current study, TLR4 and its novel endogenous ligand S100 calcium binding protein A8 (S100A8) emerged as candidate molecules involved in the progression of diabetic nephropathy by our microarray analysis performed in two different types of diabetic mouse models. Furthermore, we examined the effects of high-fat diet (HFD) feeding on streptozotocin (STZ)-induced diabetes in *Tlr4* knockout (KO) and wild-type (WT) mice in order to elucidate the mechanism for the progression of diabetic nephropathy caused by hyperlipidaemia.

Methods

Experimental animals Male *Tlr4* KO [14] and WT mice with a C57BL/6 J genetic background were studied. To generate a mouse model of diabetes complicated by hyperlipidaemia, 8-week-old mice were intraperitoneally injected with STZ (100 mg/kg body weight in citrate buffer, pH 4.0; Sigma-Aldrich, St Louis, MO, USA) or vehicle for 3 consecutive days. After 2 weeks, normal diet (ND; NMF, 14.7 kJ/g [3.5 kcal/g], 13% of energy as fat; Oriental Yeast, Tokyo, Japan) was substituted with an HFD (D12451, 19.7 kJ/g [4.7 kcal/g], 45% of energy as fat; Research Diets, New Brunswick, NJ, USA) in subgroups of animals, and all were killed for analysis at 8 weeks after STZ treatment. In another set of experiments, 8-week-old male *db/db* mice (on a BKS genetic background; Japan Clea, Tokyo, Japan) were randomly assigned to ND or HFD (D12492, 21.8 kJ/g [5.2 kcal/g], 60% of energy as fat; Research Diets) groups and followed for 4 weeks. All animal experiments were conducted in accordance with the Guidelines for Animal Research Committee of Kyoto University Graduate School of Medicine.

Human biopsy samples Human kidney samples obtained at renal biopsy carried out in our department were used for immunohistochemistry. The human study protocol was approved by the Ethical Committee on Human Research of Kyoto University Graduate School of Medicine. All participants gave written informed consent.

Measurement of metabolic variables Metabolic variables were measured as described previously [15, 16]. Briefly, blood pressure was measured by indirect tail-cuff method (Muromachi Kikai, Tokyo, Japan). Urine samples were collected with metabolism cages, and urinary albumin was measured with competitive ELISA (Exocell, Philadelphia, PA, USA). Serum and urinary creatinine levels were assayed by enzymatic method (SRL, Tokyo, Japan) [17]. Plasma glucose, triacylglycerol and total cholesterol levels were measured, under conditions of ad libitum feeding, using an enzymatic method (Wako Pure Chemicals, Osaka, Japan). Plasma insulin levels were measured by enzyme immunoassay (Morinaga, Tokyo, Japan). For measurement of tissue triacylglycerol content, lipids were extracted with isopropyl alcohol/heptane (1:1 [vol./vol.]) from frozen kidney samples. After evaporating the solvent, lipids were resuspended in 99.5% ethanol and triacylglycerol contents were measured as described above.

Real-time quantitative RT-PCR Total RNA was extracted with TRIzol reagent (Invitrogen, Carlsbad, CA, USA) and cDNA in each sample was synthesised using the High Capacity cDNA Reverse Transcription Kit (Applied Biosystems, Foster City, CA, USA) from mouse kidneys and glomeruli isolated by graded sieving method [18, 19]. TaqMan real-time PCR was performed using Premix Ex Taq (Takara Bio, Otsu, Japan) and StepOnePlus Real Time PCR System (Applied Biosystems, Foster City, CA, USA). See Electronic supplementary material (ESM) Table 1 for primer

and probe sequences. Expression levels of all genes were normalised by *Gapdh* (internal control) levels. The mean expression level in whole kidney of WT non-treated control mice was arbitrarily defined as 1.0.

Histological analysis Periodic acid–Schiff (PAS) staining of the mesangial area and immunohistochemistry of S100A8 (requiring antigen retrieval by citrate buffer) and lectin, galactoside-binding, soluble, 3 (MAC-2 or LGALS3) [18] were carried out using kidney sections (thickness 4 μm) fixed with 4% buffered paraformaldehyde. Nuclei were counterstained with haematoxylin. All the primary antibodies used in this study are shown in ESM Table 2. For double staining, primary antibody for S100A8 was visualised with DyLight-conjugated secondary antibody (Takara Bio, Otsu, Japan). Immunofluorescence of podocin (or NPHS2) was performed with snap-frozen cryostat sections (4 μm), pretreated with cold acetone and 0.1% Triton-X100, and with primary and FITC-labelled secondary antibodies. Photographs were taken by a fluorescence microscope (IX81-PAFM; Olympus, Tokyo, Japan). Mesangial and podocin-positive areas of more than ten glomeruli from the outer cortex were measured quantitatively to obtain an average for each mouse using MetaMorph 7.5 software (Molecular Devices, Downingtown, PA, USA). Formalin-fixed, snap-frozen sections (10 μm) were stained with Oil Red O to evaluate lipid-droplet-positive areas.

Microarray analysis Two different types of diabetic mouse model were employed for microarray analysis. Male A-ZIP/F-1 heterozygous transgenic mice and control male FVB/N littermates were used at 10 months of age, when A-ZIP/F-1 mice exhibited diabetic nephropathy with massive proteinuria [20]. The other model was STZ-induced, insulin-dependent, diabetic C57BL/6 J male mice (Japan Clea) in which diabetes was induced at 9 weeks of age by single intraperitoneal injection of STZ (180 mg/kg); mice were analysed 8 weeks later. We essentially followed the procedures described in detail in the GeneChip Eukaryotic Target Preparation & Hybridization Manual (Affymetrix, Santa Clara, CA, USA). In brief, cDNA was synthesised and biotin-labelled cRNA was produced through in vitro transcription labelling Kit (Affymetrix). Fragmented cRNA was hybridised to GeneChip Mouse Genome 430 2.0 Array (Affymetrix) at 45°C for 16 h. The samples were washed and stained according to the manufacturer's protocol on GeneChip Fludisc Station 450 (Affymetrix) and scanned on GeneChip Scanner 3000 (Affymetrix).

PCR array analysis To eliminate contaminating genomic DNA, total RNA extracted from kidney samples was purified using RNeasy Mini Kit (QIAGEN Sciences, Maryland, MD, USA). First-strand cDNA was synthesised from total RNA using the RT2 first-strand kit (SABiosciences, Frederick, MD, USA). The mouse TLR-signalling pathway RT2 Profiler PCR plate (PAMM-018, SABiosciences) and StepOnePlus were used for amplification of cDNA. The analysis used 96 well plates containing gene-specific primer sets for 84 relevant TLR pathway genes, five housekeeping genes and two negative controls. The cycle threshold (C_t) was determined for each sample and normalised to the average C_t of the five housekeeping genes. The comparative ΔC_t method (SABiosciences) was used to calculate relative gene expression.

Western blot analysis Proteins extracted from kidney samples were separated by SDS-PAGE, transferred onto PVDF membranes, incubated with primary antibodies and detected with peroxidase-conjugated secondary antibodies and chemiluminescence [19]. Glyceraldehyde-3-phosphate dehydrogenase (GAPDH) was used as an internal control.

Cultured macrophages Palmitate (Sigma-Aldrich) was solubilised in ethanol, and combined with fatty-acid-free, low endotoxin, bovine serum albumin (Sigma-Aldrich) at a molar ratio of 10:1 in serum-free medium. Polymyxin B (10 μg/ml, Nacalai Tesque, Kyoto, Japan) was added to each well to minimise contamination of endotoxin. Bone marrow-derived macrophages (BMDMs) were generated from mice as described previously [21]. Briefly, following lysis of erythrocytes, bone marrow cells were resuspended in medium containing 20% fetal calf serum and 50 ng/ml recombinant human macrophage colony-stimulating factor, and cultured at 37°C in 5% CO_2 atmosphere. On day 6, the medium was replaced with fresh medium containing 5.6 mmol/l or 25 mmol/l glucose. On day 7, macrophages were incubated with palmitate or vehicle for 24 h. Total RNA from cells was extracted with RNeasy Mini Kit, and mRNA expression levels of *S100a8* and *Tlr4* were determined by TaqMan real-time RT-PCR.

Statistical analysis Data are expressed as means±SEM. Differences between multiple groups were assessed by two-way factorial ANOVA with Bonferroni's post test. Comparisons between two groups were carried out by unpaired Student's *t* test. Statistical significance was defined as $p<0.05$.

Results

Changes of metabolic variables and albuminuria in WT diabetic mice given a fat-rich diet Metabolic variables of non-STZ (nSTZ)-HFD, STZ-ND, STZ-HFD and control nSTZ-ND groups of WT mice are shown in Table 1. HFD treatment (compared with ND) in nSTZ mice caused significant elevation of body weight, plasma glucose, insulin,

Table 1 Metabolic data of WT and *Tlr4* KO mice at 8 weeks after STZ injection

Variable	WT				KO			
	nSTZ-ND	nSTZ-HFD	STZ-ND	STZ-HFD	nSTZ-ND	nSTZ-HFD	STZ-ND	STZ-HFD
Number of animals	6	4	8	11	4	4	5	8
Body weight (g)	27.7±1.0	33.7±0.5**	20.0±0.9**	22.1±0.5**,§§§	34.9±2.4†	39.6±1.4†	22.0±1.3**	23.3±0.6***,§§§
Blood pressure (mmHg)								
Systolic	101±2	104±2	98±1	100±1	103±2	103±2	96±1*	101±2
Diastolic	56±2	57±3	52±2	56±2	55±1	57±2	50±1*	53±1
Kidney weight (% body weight)	0.5±0.0	1.0±0.0**	1.7±0.1**	1.8±0.1**,§§§	1.0±0.1†††	2.2±0.2***,††	1.9±0.2***	1.9±0.1***
Plasma glucose (mmol/l)	9.5±1.6	14.0±0.4*	40.0±3.9**	32.9±1.8**,§	10.4±1.1	12.7±2.3	36.0±7.7*	31.8±2.3***,§§
HbA_{1c} (%)	3.4±0.1	5.3±0.1**	9.6±0.6**	9.9±0.5**,§	3.0±0.3	4.9±0.2**	9.4±1.1**	10.3±0.3***,§§§
HbA_{1c} (mmol/mol)	13.3±1.4	34.1±0.7**	81.8±6.5**	84.6±5.1**,§	9.0±2.8	29.5±2.5**	78.9±12.5**	89.4±3.2***,§§§
Plasma insulin (pmol/l)	133±16	256±21**	10±2**	12±2**,§§§	238±43	336±33	12±5**	12±5**,§§§
Plasma triacylglycerol (mmol/l)	0.99±0.02	1.20±0.03**	2.36±1.01*	5.48±1.56*,§	1.74±0.32	1.42±0.11	3.12±1.56	7.64±1.58**,§§
Plasma total cholesterol (mmol/l)	1.5±0.4	3.4±0.3*	5.1±0.8*	5.2±0.5**	1.9±0.4	3.4±0.2*	3.8±0.6*	5.9±0.4**,§§,‡
Serum creatinine (μmol/l)	8.0±1.8	8.8±0.1	10.6±0.9	15.9±5.3	8.8±0.1	8.0±0.1††	10.6±1.8	8.0±0.1

Data are means±SEM

Blood was collected with mice fed ad libitum

*$p<0.05$, **$p<0.01$, ***$p<0.001$ vs nSTZ-ND; †$p<0.05$, ††$p<0.01$, †††$p<0.001$ vs similarly treated group of WT; ‡$p<0.05$ vs STZ-ND; §$p<0.05$, §§$p<0.01$, §§§$p<0.001$ vs nSTZ-HFD

triacylglycerol and total cholesterol levels. STZ treatment (compared with nSTZ) in ND mice caused significant body weight loss and significant elevation of plasma glucose, triacylglycerol and total cholesterol levels. Treatment of STZ mice with HFD resulted in large exacerbation of hypertriacylglycerolaemia (by 2.3-fold) without significant changes in other above-mentioned variables (Table 1). Consistently, renal lipid deposition in STZ-HFD mice was markedly increased compared with STZ-ND mice (Fig. 1a, b). Blood pressures were not significantly different among the four treatment groups (Table 1).

Concerning albuminuria, one of the representative abnormalities that characterise diabetic nephropathy [2], albumin excretion in STZ-ND was elevated by 2.3-fold at 8 weeks compared with nSTZ-ND mice (Fig. 1c). The addition of HFD to STZ mice further enhanced albuminuria approximately twofold. To investigate podocyte injury, we investigated whether podocin protein production is decreased in the glomeruli of STZ-HFD mice [19]. Glomerular podocin level was significantly reduced in STZ-ND compared with nSTZ-ND and was lowest in STZ-HFD (Fig. 1e, f). Also, in obese, type 2 diabetic *db/db* mice, albuminuria was exaggerated by HFD (ESM Fig. 1). To summarise, treatment of WT mice with a combination of HFD and STZ resulted in marked enhancement of hypertriglycerolaemia, renal lipid deposition, podocyte damage and albumin excretion.

Gene expression analysis of pro-inflammatory and extracellular-matrix-associated genes in whole kidney and glomeruli and histological examination We measured mRNA levels of pro-inflammatory and extracellular matrix (ECM)-associated genes both in whole kidney and isolated glomeruli (Fig. 2, ESM Table 3). The former set of genes included *Mcp1* (also known as *Ccl2*, encoding monocyte chemoattractant protein-1 [MCP1]), *F4/80* (also known as *Emr1*), *Cd68*, *Tnfa* (also known as *Tnf* [encoding TNF]), *Pai1* (also known as *Serpine1* [encoding plasminogen activator inhibitor-1]) and *Il1b* (encoding IL1β). The latter set comprised *Tgfb1* (encoding TGFβ1), *Fn* (also known as *Fn1* [encoding fibronectin]), *Col4a3* (encoding type IV collagen alpha 3 chain), *Ctgf* (encoding connective tissue growth factor [CTGF]) and *Mmp2* (encoding matrix metalloproteinase 2). We found that expression levels of these genes in glomeruli and whole kidney were mildly elevated in WT STZ-ND compared with WT nSTZ-ND mice, in general (Fig. 2, ESM Table 3). Gene expression levels were further upregulated in WT STZ-HFD animals. Of note, differences between nSTZ-HFD and nSTZ-ND groups were

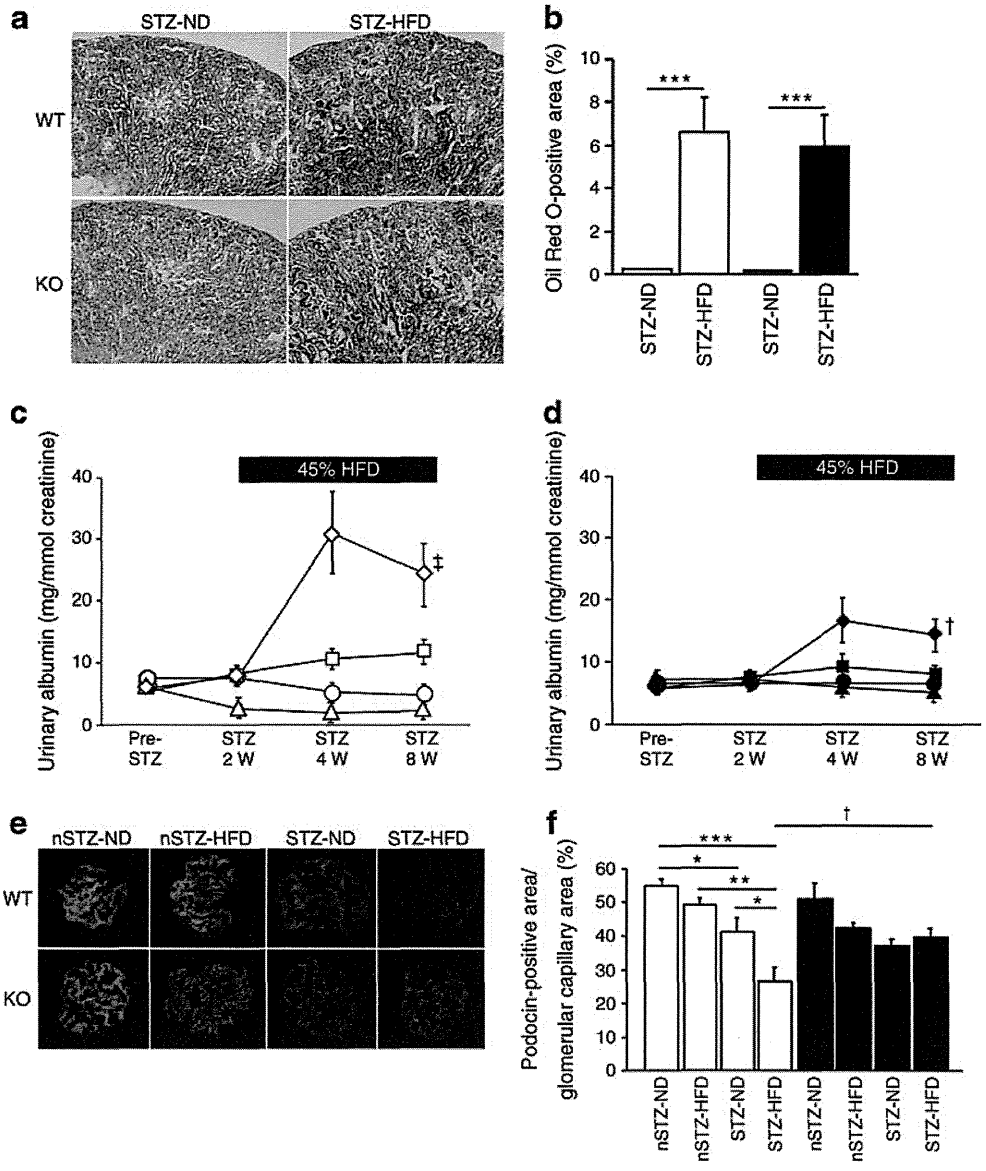

Fig. 1 Treatment of STZ diabetic mice with an HFD worsens renal injury in WT but not in *Tlr4* KO mice. (**a**, **b**) Addition of HFD to STZ mice causes similar degrees of deposition of lipid droplets staining positive with Oil Red O in WT (white bars) and KO mice (black bars) at 16 weeks of age. Magnification×4. Data are means±SEM. $n=5$. ***$p<0.001$. Time course of urinary albumin levels normalised with urinary creatinine levels in WT (**c**) and *Tlr4* KO mice (**d**). Circles, nSTZ-ND; triangles, nSTZ-HFD; squares, STZ-ND; diamonds, STZ-HFD. W, weeks after STZ injection. $n=6$–10. $^{‡}p<0.05$ vs WT STZ-ND, $^{†}p<0.05$ vs WT STZ-HFD calculated by area under the curve. (**e**, **f**) Immunofluorescence analysis of glomerular podocin level. White bars, WT; black bars, KO; $n=4$–6. *$p<0.05$, **$p<0.01$, ***$p<0.001$. $^{†}p<0.05$ for similarly treated KO vs WT

negligible (Fig. 2). Histological analysis also showed that MAC-2-positive-macrophage infiltration into glomeruli (Fig. 3a) and renal interstitium (ESM Fig. 2) and glomerular mesangial expansion (Fig. 3b) in STZ-HFD mice were markedly more pronounced than in STZ-ND mice.

Screening of candidate genes involved in the pathogenesis of diabetic nephropathy To identify candidate molecules potentially involved in the pathophysiology of diabetic nephropathy, we analysed gene expression profiles of diabetic mouse glomeruli by microarray (ESM Table 4). We compared two types of diabetic nephropathy from STZ-induced and A-ZIP/F-1 lipoatrophic diabetes mice. We selected commonly regulated genes to minimise interference from the renal toxicity of STZ, genetic background [22] and direct insulin or leptin target molecules [23]. The list of genes commonly upregulated in these two models included pro-inflammatory and ECM-associated genes and also ones encoding TLRs (ESM Table 4). As pairs of cell surface receptors and their ligands provide attractive seeds for future therapeutic targets, we focused on TLR4, for which glomerular levels were elevated by 1.7-fold by STZ and 5.8-fold in A-ZIP/F-1 compared with each control by microarray. We further examined the expression of genes encoding molecules reported to be endogenous ligands for TLR4 [7], and identified *S100a8* (also known as *Mrp8*) and *S100a9* (also known as *Mrp14*]) [24], for which glomerular gene expression was commonly upregulated in two models of diabetic nephropathy by microarray (ESM Table 4). Upregulation of *Tlr4* and *S100a8* gene expression in glomeruli of STZ and A-ZIP/F-1 mice was confirmed by quantitative RT-PCR (ESM Fig. 3a, b). Moreover, in STZ-HFD mice, expression of these genes was further potentiated compared with other groups such as STZ-ND and nSTZ-HFD, especially in

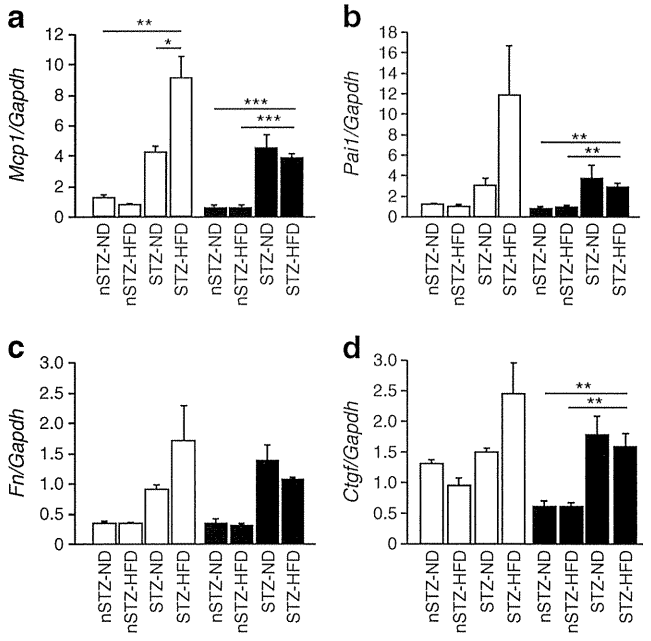

Fig. 2 Treatment with STZ and HFD synergistically upregulates inflammatory and ECM-associated gene expression in glomeruli of WT mice by real-time RT-PCR, but the effects of HFD are largely blunted in *Tlr4* KO mice: (**a**) *Mcp1*; (**b**) *Pai1*; (**c**) *Fn*; and (**d**) *Ctgf*. White bars, WT; black bars, KO. Data are means±SEM. n=4–11. *p<0.05, **p<0.01, ***p<0.001

glomeruli (Fig. 4a), but not in whole kidney (ESM Fig. 4). However, there was no significant increase in the expression of genes encoding other endogenous ligands for TLR4, such as *Hmgb1*, at the same time in both STZ and A-ZIP/F-1 mice compared with their respective controls, as assessed by microarray (ESM Table 4) or by quantitative RT-PCR (ESM Fig. 3c, d).

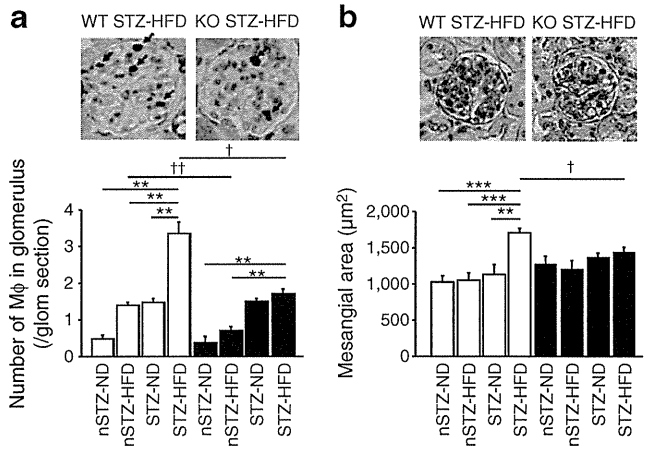

Fig. 3 Glomerular macrophage infiltration and mesangial matrix accumulation are markedly enhanced in WT mice co-treated with STZ and HFD, but not in *Tlr4* KO mice. **a** Macrophage (Mϕ) number per glomerular (glom) section determined by MAC-2 immunostaining (arrows). Magnification ×40. Data are means±SEM. n=4–5. **b** Glomerular mesangial area determined by PAS staining (purple). Magnification ×20. n=4–6. White bars, WT; black bars, KO. **p<0.01, ***p<0.001. $^{\dagger}p$<0.05, $^{\dagger\dagger}p$<0.01 for similarly treated KO vs WT

Production of S100A8 protein in diabetic kidney We performed immunohistochemical analyses of S100A8 protein in the kidneys both in STZ-HFD mice and human biopsy samples. In mice, abundance of S100A8 protein, in a punctate pattern, was observed predominantly in glomeruli of WT STZ-HFD mice, while S100A8 abundance was much lower in glomeruli of nSTZ-ND, nSTZ-HFD and STZ-ND groups (Fig. 4b, ESM Fig. 5). S100A8 protein was also detected in the interstitium of STZ-HFD mice but less abundantly than in the glomeruli. Double immunostaining revealed that 86% of S100A8 signals co-localised with macrophage marker MAC-2 in the glomeruli of STZ-HFD mice (Fig. 4c). In humans, S100A8 was abundantly detected in the glomeruli of patients with diabetic nephropathy, but not obviously in glomeruli of minor glomerular abnormality or minimal change nephrotic syndrome cases (Fig. 5).

Effects of Tlr4 defect on STZ-HFD mice and on BMDMs To elucidate a functional role played by TLR4 in the progression of diabetic nephropathy accelerated by diet-induced hyperlipidaemia, we investigated the effects of STZ and HFD in *Tlr4* KO mice. In baseline nSTZ-ND conditions, KO mice showed significantly heavier body weights compared with WT mice, paralleled by mildly elevated plasma levels of glucose, insulin, triacylglycerol and total cholesterol in KO mice (Table 1). Plasma glucose levels in KO nSTZ-HFD mice were slightly lower compared with their WT counterparts. These findings are consistent with previous observations indicating that, compared with WT mice, *Tlr4* KO mice are prone to accumulation of fat but resistant to development of insulin resistance when challenged with an HFD [25, 26]. When STZ-HFD conditions were compared between KO and WT mice, the levels of plasma glucose and total cholesterol and renal lipid deposition were similar among the genotypes, and plasma triacylglycerol levels tended to be higher in KO than WT mice (Table 1, Fig. 1b). On the other hand, exacerbation of albuminuria and suppression of glomerular podocin protein production resulting from HFD treatment in WT STZ mice were all largely blunted in KO STZ animals (Fig. 1c–f). Additionally, infiltrated macrophage counts in glomeruli and renal interstitium and mesangial expansion were remarkably smaller in KO STZ-HFD mice than in WT STZ-HFD mice (Fig. 3, ESM Fig. 2). Furthermore, upregulation of pro-inflammatory (*Mcp1* and *Pai1*), pro-fibrotic (*Fn* and *Ctgf*), *S100a8* and *S100a9* gene expression and S100A8-positive cell counts caused by HFD treatment in glomeruli of WT STZ mice were almost completely abolished in KO STZ mice (Figs 2 and 4a, b, ESM Fig. 5). These findings indicate that, despite similar degrees of metabolic abnormalities caused

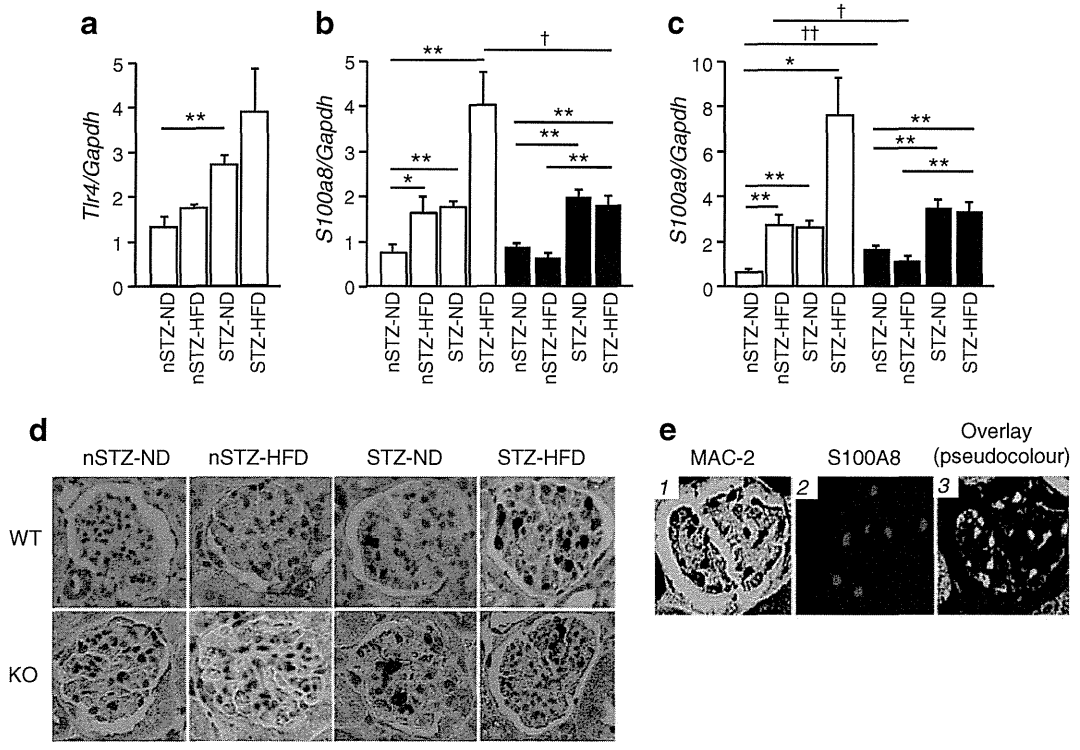

Fig. 4 Glomerular expression of *Tlr4*, *S100a8* and *S100a9* mRNA and S100A8 protein is markedly upregulated in WT STZ-HFD but not in *Tlr4* KO STZ-HFD mice, and S100A8 is predominantly produced by glomerular macrophages in WT STZ-HFD mice. **a–c** Gene expression of *Tlr4* (**a**), *S100a8* (**b**) and *S100a9* (**c**) in glomeruli, determined by real-time RT-PCR. White bars, WT; black bars, KO. Data are means± SEM. n=4–11. *p<0.05, **p<0.01. $^{\dagger}p$<0.05, $^{\dagger\dagger}p$<0.01 for similarly treated KO vs WT. **d** Glomerular S100A8 protein (brown) examined by immunohistochemistry. Magnification×40. **e** Localisation of MAC-2 (brown in panel 1, pseudocoloured with green in panel 3, by immunohistochemistry), S100A8 (red in panels 2 and 3, by immunofluorescence) and their overlaps (yellow in panel 3) in glomeruli of WT STZ-HFD mice

by diabetes and hyperlipidaemia, *Tlr4* KO mice developed much less severe renal lesions compared with WT mice.

With regard to comparison between WT and *Tlr4* KO mice treated with STZ alone (STZ-ND mice), urinary albumin excretion (Fig. 1c, d), glomerular podocin production (Fig. 1e, f), glomerular gene expression of *Mcp1*, *Pai1*, *Fn*, *Ctgf*, *S100a8*, and *S100a9* (Figs 2 and 4a), and glomerular macrophage infiltration (Fig. 3a) were all similar among two genotypes, suggesting that *Tlr4* does not strongly participate in early and mild changes of diabetic nephropathy. Concerning HFD treatment alone (nSTZ-HFD mice), there were no significant differences in urinary albumin excretion and glomerular podocin production between WT and KO mice (Fig. 1c–f), while glomerular *S100a9* gene expression (Fig. 4a) and glomerular macrophage infiltration (Fig. 3a) were significantly attenuated in KO compared with WT mice, suggesting that treatment solely with HFD significantly activated circulating macrophages in WT mice but the TLR4-mediated signal in nSTZ-HFD mice was not sufficient to cause functional changes in the glomeruli.

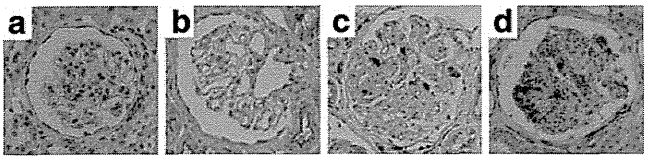

Fig. 5 S100A8 (brown) is observed in glomeruli of patients with diabetic nephropathy by immunohistochemistry: (**a**) minor glomerular abnormality; (**b**) minimal change nephrotic syndrome; and (**c**) mild and (**d**) severe cases of diabetic nephropathy

To gain insights into how the combination of diabetes and hyperlipidaemia resulted in markedly enhanced migration of macrophages into glomeruli, we examined BMDMs. We focused attention on expression of a potent TLR4 ligand, S100A8 [24]. Treatment of WT macrophages with a fatty acid, palmitate, induced *S100a8* mRNA upregulation when the cells were cultured in high-glucose conditions, but upregulation was not observed under low-glucose conditions (Fig. 6a). Furthermore, induction of *S100a8* expression by palmitate in high-glucose-treated macrophages did not occur in cells from *Tlr4* KO animals (Fig. 6b). High-glucose treatment slightly increased *Tlr4* expression in WT macrophages (Fig. 6c).

TLR4 signalling in the kidney of STZ-HFD model To examine the TLR4-downstream signalling cascade, we performed

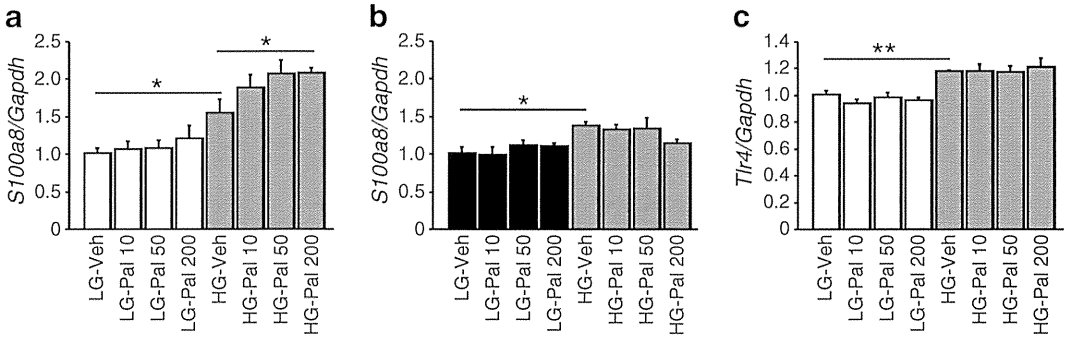

Fig. 6 *S100a8* expression in BMDMs is synergistically induced by high glucose and palmitate in a *Tlr4*-dependent manner. **a** *S100a8* mRNA expression by real-time RT-PCR in BMDMs from WT mice cultured under low-glucose (5.6 mmol/l, white bars) or high-glucose (25 mmol/l, grey bars) conditions and effects of palmitate (10–200 μmol/l). Data are means±SEM. $n=6$. **b** *S100a8* mRNA expression in BMDMs from *Tlr4* KO mice cultured under low-glucose (black bars) or high-glucose (grey bars) conditions and the effects of palmitate. $n=6$. **c** *Tlr4* mRNA expression in WT BMDMs. $n=6$. *$p<0.05$, **$p<0.01$. LG, low glucose; HG, high glucose; pal, palmitate; Veh, vehicle

western blot analyses of key adaptor proteins and transcription factors which have been reportedly classified into myeloid differentiation primary response gene (88) (MYD88)-dependent, TIR-domain-containing adapter-inducing interferon-β (TRIF)-dependent or common pathways (Fig. 7a) [7], using whole kidney lysate. Treatment of WT STZ mice with HFD was associated with increased phosphorylation of inhibitor of κB (IKB) and c-Jun N-terminal kinase (JNK) in a common pathway, and with increased phosphorylation of interferon regulatory factor 3 (IRF3) in a TRIF-dependent pathway, but not with increased protein production of TNF receptor-associated factor 6 (TRAF6) nor increased phosphorylation of interleukin-1-receptor-associated kinase (IRAK) in the MYD88-dependent pathway (Fig. 7b–e). PCR array analysis, which allows simultaneous evaluation of relevant genes involved in the signalling cascades of TLR1–TLR9, confirmed that in WT STZ-HFD kidneys, TRIF-dependent pathway-inducible genes (*Cxcl10*, *Ifnb1* [encoding interferon β1] and *Cd80*) and common pathway-inducible genes (*Mcp1*) were highly upregulated, but genes involved in the MYD88-dependent pathway (*Cd14*, *Ly96* [encoding myeloid differentiation protein-2 {MD-2}], and *Traf6*) were not changed compared with WT STZ-ND kidneys (ESM Table 5). Furthermore, disruption of the *Tlr4* gene markedly blocked the activation of the putative TLR4 downstream signalling cascade in STZ-HFD mice (Fig. 7b–e, ESM Table 5).

Discussion

In the present study, we have revealed that treatment of WT mice with STZ combined with HFD synergistically aggravated renal lesions, indicated by enhancement of albuminuria, macrophage infiltration, mesangial expansion and pro-inflammatory/ECM-associated gene induction in glomeruli. These changes were accompanied with upregulation of a TLR4 ligand, S100A8, and activation of putative TRIF-dependent pathway downstream of TLR4. In *Tlr4* KO mice, the addition of HFD to STZ had almost no effect on kidney damage, suggesting that TLR4 plays an important role in the exacerbation of diabetic nephropathy by hyperlipidaemia.

Of note, treatment with STZ alone caused similar and mild renal changes in WT and KO mice, suggesting that the TLR4 signal may not significantly participate in the onset of diabetic nephropathy at 8 weeks after STZ injection [13]. However, WT mice fed with HFD (nSTZ-HFD) exhibited significantly higher levels of *S100a9* gene expression and more macrophage infiltration in glomeruli compared with KO mice, but these effects were not reflected in differences in other renal lesion variables, suggesting that macrophage activation in nSTZ-HFD mice may require longer observation periods than were used in this study in order to be functionally relevant.

Here, to study the effects of an HFD on diabetes, we used a lean model of type 1 diabetes to avoid introducing complexity through alterations in insulin resistance and fat accumulation with the HFD or by *Tlr4* gene disruption in the type 2 diabetes model [19, 20]. The HFD-induced and hypertriacylglycerolaemia-associated renal injury observed in this study may have been caused through activation of TLR4 by NEFA [25, 26], oxidised LDL [27], or triacylglycerol-rich lipoproteins [6]. Previous studies have proposed that, by direct lipotoxicity on tubular epithelial cells, diet-induced obesity alone is sufficient to cause inflammatory and fibrotic changes in the whole kidney preparations through gene expression of *Cd36* or *sterol regulatory element-binding protein-1c* (*Srebp1c*) [28–30]. In the present study, however, treatment of WT mice solely with HFD resulted in very mild renal lesions, probably because we used a diet with a lower fat content and studied the mice for a shorter period of time compared with earlier reports [28–30]. Furthermore, HFD increased glomerular *Cd36* mRNA expression but STZ-induced

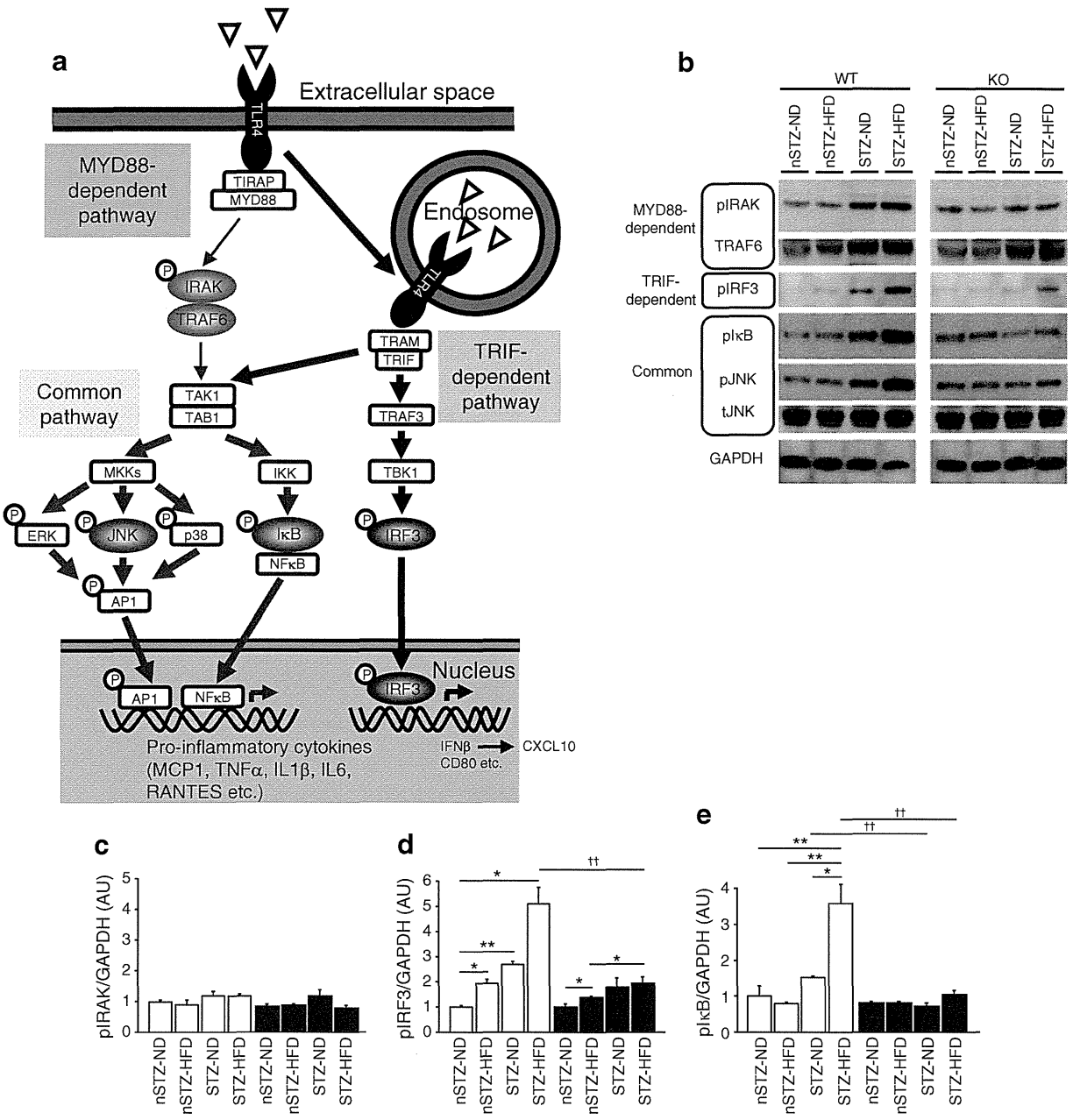

Fig. 7 Exacerbation of STZ-induced diabetic nephropathy by HFD is associated with increased phosphorylation of proteins involved in TRIF-dependent and common pathways of the TLR4 signalling cascade in WT kidney but not in *Tlr4* KO kidney. **a** Schema describing the known TLR4 signalling cascade. The common pathway can be activated both through MYD88-dependent and TRIF-dependent pathways. Key molecules analysed in (b) are highlighted as elliptical objects. **b-e** Western blot analyses of TLR4 signalling and quantitative evaluation. White bars, WT; black bars, KO. Data are means±SEM. $n=4$. *$p<0.05$, **$p<0.01$. $^{\dagger\dagger}p<0.01$ for similarly treated KO vs WT. AP1, jun proto-oncogene; AU, arbitrary units; CXCL10, chemokine (C-X-C motif) ligand 10; ERK, mitogen-activated protein kinase 1; (p)IKB, (phosphorylated) inhibitor of κB ; IKK, inhibitor of kappa light polypeptide gene enhancer in B cells, kinase; (p)IRAK, (phosphorylated) interleukin-1 receptor-associated kinase 1; pIRF3, phosphorylated IRF3; (p)/(t)JNK, (phosphorylated)/(total) JNK; MKKs, mitogen-activated protein kinase kinases; p38, mitogen-activated protein kinase 14; RANTES, chemokine (C-C motif) ligand 5; TAB1, TGFβ-activated kinase 1/MAP3K7 binding protein 1; TAK1, nuclear receptor subfamily 2, group C, member 2; TBK1, TANK-binding kinase 1; TIRAP, Toll-interleukin 1 receptor domain containing adaptor protein; TRAF3, TNF receptor-associated factor 3; TRAM, translocation associated membrane protein 1

diabetes reduced it, and glomerular *Srebp1c* expression was decreased both by HFD and STZ (ESM Fig. 6), indicating that HFD-induced exacerbation of diabetic nephropathy cannot be explained by upregulation of CD36 or SREBP1C.

S100A8 forms a heterodimer with S100A9, and the complex is one of the most powerful endogenous ligands for TLR4, which is essential for full activation of macrophages and other leucocytes, by a positive feedback loop, during

endotoxin-induced shock and vascular and autoimmune disorders [24, 31, 32]. TLR4 signalling also plays an important role in the development of various kidney diseases, yet the role of TLR4 in diabetic glomerulopathy or hyperlipidaemia-induced kidney damage remains to be elucidated [8–13]. Recently, Burkhardt et al and Bouma et al reported that serum S100A8/A9 complex concentrations were elevated in patients with diabetes [33, 34]. In our study, S100A8 protein was abundant in the glomeruli of mice given STZ and HFD and also in glomeruli of patients with diabetic nephropathy, and was mainly produced by macrophages. Furthermore, we found that high glucose and NEFA treatments, when combined, markedly upregulated *S100a8* expression in WT macrophages, but not in *Tlr4* KO macrophages. These findings suggest that production of S100A8 is not just an indicator of systemic inflammation but may play a pathogenic role in the deterioration of diabetic nephropathy. Functional analysis of S100A8 protein production in diabetic mice is currently under way in our laboratory. Candidate *Tlr4*-expressing cells in the diabetic kidney include macrophages, podocytes and mesangial and tubular epithelial cells [8, 9]. So far, we have been unable to obtain reliable findings by immunohistochemistry using commercially available antibodies for TLR4, and we are now trying other methods. Of note, upregulation of *S100a8* gene expression by HFD in STZ mice was also observed in the liver and aorta, suggesting that the effects of these treatments are not specifically targeted to the kidney but are systemic (ESM Fig. 6). HMGB1 is one of endogenous ligands of TLR4 [9], and AGE-specific receptor (AGER or RAGE) is one of the S100A8 receptors so far identified [35]. Although mRNA expression of these molecules in glomeruli was not upregulated in diabetic mice in this study (ESM Fig. 3, ESM Table 4), we cannot exclude the possibility that they are involved in hyperlipidaemia-induced renal injury.

The macrophage has been presumed to be a critical mediator of diabetic nephropathy [36–38], and blockade of the MCP-1/CC chemokine receptor 2 system in diabetic mice leads to reduced albuminuria, mesangial expansion and macrophage infiltration [39–42]. Secretory factors from macrophages may cause histological and functional changes in glomeruli. For example, TGF β1 (TGFB1) and MCP1, induced in surrounding cells by or secreted directly from activated macrophages, have been shown to upregulate CTGF production [43] and increase albumin permeability in cultured podocytes [44–46]; we have recently reported that overproduction of CTGF specifically in podocytes is sufficient to worsen diabetic nephropathy [19].

Downstream signalling of TLR4 has been divided into MYD88-dependent and TRIF-dependent pathways, leading to early- and late-phase nuclear factor of κ light polypeptide gene enhancer in B cells 1 (NFκB) activation, respectively [7]. In addition, endocytosed TLR4 activates the TRIF-dependent pathway [47]. It is interesting to determine whether pathologically accumulated lipids in endosomes of macrophages can cause chronic inflammation via the TRIF-dependent pathway in the kidneys of STZ-HFD mice. Here, in STZ-HFD kidneys, we observed an increase in IRF3 protein phosphorylation and *Cxcl10*, *Ifnb1* and *Cd80* mRNA expression, reported to be in the TRIF-dependent pathway, but experiments blocking TRIF activity are required to demonstrate the TRIF dependency of the process.

In conclusion, we have elucidated a novel mechanism of hyperlipidaemia-induced renal damage in diabetic conditions in a TLR4-dependent manner that appears to involve the activation of a S100A8/TLR4 signalling pathway in glomeruli. Further investigation is required to see whether this signalling cascade is relevant in the progression of nephropathy in diabetic patients.

Acknowledgements We acknowledge S. Akira (WPI Immunology Frontier Research Center, Osaka University, Suita, Japan) for kindly providing us with *Tlr4* KO mice. We gratefully acknowledge Y. Ogawa and A. Yamamoto and other laboratory members for their assistance.

Funding This work was supported in part by Grant-in-Aid for Diabetic Nephropathy Research (K. Mori), research grants from the Japanese Ministry of Education, Culture, Sports, Science and Technology (T. Kuwabara, K. Mori and M. Mukoyama) and from the Smoking Research Foundation (M. Mukoyama).

Duality of interest The authors declare that there is no duality of interest associated with this manuscript.

Contribution statement All authors contributed to the conception and design, or analysis and interpretation of data, and drafting the article or revising it critically for important intellectual content, and have given final approval of the version to be published.

References

1. Maisonneuve P, Agodoa L, Gellert R et al (2000) Distribution of primary renal diseases leading to end-stage renal failure in the United States, Europe, and Australia/New Zealand: results from an international comparative study. Am J Kidney Dis 35:157–165
2. Decleves AE, Sharma K (2010) New pharmacological treatments for improving renal outcomes in diabetes. Nat Rev Nephrol 6:371–380
3. El-Atat FA, Stas SN, McFarlane SI, Sowers JR (2004) The relationship between hyperinsulinemia, hypertension and progressive renal disease. J Am Soc Nephrol 15:2816–2827
4. Perkins BA, Ficociello LH, Silva KH, Finkelstein DM, Warram JH, Krolewski AS (2003) Regression of microalbuminuria in type 1 diabetes. N Engl J Med 348:2285–2293
5. Ravid M, Brosh D, Ravid-Safran D, Levy Z, Rachmani R (1998) Main risk factors for nephropathy in type 2 diabetes mellitus are plasma cholesterol levels, mean blood pressure, and hyperglycemia. Arch Intern Med 158:998–1004
6. Rutledge JC, Ng KF, Aung HH, Wilson DW (2010) Role of triglyceride-rich lipoproteins in diabetic nephropathy. Nat Rev Nephrol 6:361–370

7. Akira S, Takeda K (2004) Toll-like receptor signalling. Nat Rev Immunol 4:499–511
8. Brown HJ, Lock HR, Wolfs TG, Buurman WA, Sacks SH, Robson MG (2007) Toll-like receptor 4 ligation on intrinsic renal cells contributes to the induction of antibody-mediated glomerulonephritis via CXCL1 and CXCL2. J Am Soc Nephrol 18:1732–1739
9. Wu H, Chen G, Wyburn KR et al (2007) TLR4 activation mediates kidney ischemia/reperfusion injury. J Clin Invest 117:2847–2859
10. Zhang B, Ramesh G, Uematsu S, Akira S, Reeves WB (2008) TLR4 signaling mediates inflammation and tissue injury in nephrotoxicity. J Am Soc Nephrol 19:923–932
11. Liu B, Yang Y, Dai J et al (2006) TLR4 up-regulation at protein or gene level is pathogenic for lupus-like autoimmune disease. J Immunol 177:6880–6888
12. Kruger B, Krick S, Dhillon N et al (2009) Donor Toll-like receptor 4 contributes to ischemia and reperfusion injury following human kidney transplantation. Proc Natl Acad Sci USA 106:3390–3395
13. Lin M, Yiu WH, Wu HJ et al (2012) Toll-like receptor 4 promotes tubular inflammation in diabetic nephropathy. J Am Soc Nephrol 23:86–102
14. Hoshino K, Takeuchi O, Kawai T et al (1999) Cutting edge: Toll-like receptor 4 (TLR4)-deficient mice are hyporesponsive to lipopolysaccharide: evidence for TLR4 as the Lps gene product. J Immunol 162:3749–3752
15. Kuwabara T, Mori K, Mukoyama M et al (2009) Urinary neutrophil gelatinase-associated lipocalin levels reflect damage to glomeruli, proximal tubules, and distal nephrons. Kidney Int 75:285–294
16. Kusakabe T, Tanioka H, Ebihara K et al (2009) Beneficial effects of leptin on glycaemic and lipid control in a mouse model of type 2 diabetes with increased adiposity induced by streptozotocin and a high-fat diet. Diabetologia 52:675–683
17. Jung K, Wesslau C, Priem F, Schreiber G, Zubek A (1987) Specific creatinine determination in laboratory animals using the new enzymatic test kit "Creatinine-PAP". J Clin Chem Clin Biochem 25:357–361
18. Suganami T, Mukoyama M, Sugawara A et al (2001) Overexpression of brain natriuretic peptide in mice ameliorates immune-mediated renal injury. J Am Soc Nephrol 12:2652–2663
19. Yokoi H, Mukoyama M, Mori K et al (2008) Overexpression of connective tissue growth factor in podocytes worsens diabetic nephropathy in mice. Kidney Int 73:446–455
20. Suganami T, Mukoyama M, Mori K (2005) Prevention and reversal of renal injury by leptin in a new mouse model of diabetic nephropathy. FASEB J 19:127–129
21. Suganami T, Yuan X, Shimoda Y et al (2009) Activating transcription factor 3 constitutes a negative feedback mechanism that attenuates saturated Fatty acid/toll-like receptor 4 signaling and macrophage activation in obese adipose tissue. Circ Res 105:25–32
22. Qi Z, Fujita H, Jin J et al (2005) Characterization of susceptibility of inbred mouse strains to diabetic nephropathy. Diabetes 54:2628–2637
23. Vaisse C, Halaas JL, Horvath CM, Darnell JE Jr, Stoffel M, Friedman JM (1996) Leptin activation of Stat3 in the hypothalamus of wild-type and ob/ob mice but not db/db mice. Nat Genet 14:95–97
24. Vogl T, Tenbrock K, Ludwig S et al (2007) Mrp8 and Mrp14 are endogenous activators of Toll-like receptor 4, promoting lethal, endotoxin-induced shock. Nat Med 13:1042–1049
25. Suganami T, Mieda T, Itoh M, Shimoda Y, Kamei Y, Ogawa Y (2007) Attenuation of obesity-induced adipose tissue inflammation in C3H/HeJ mice carrying a Toll-like receptor 4 mutation. Biochem Biophys Res Commun 354:45–49
26. Shi H, Kokoeva MV, Inouye K, Tzameli I, Yin H, Flier JS (2006) TLR4 links innate immunity and fatty acid-induced insulin resistance. J Clin Invest 116:3015–3025
27. Xu XH, Shah PK, Faure E et al (2001) Toll-like receptor-4 is expressed by macrophages in murine and human lipid-rich atherosclerotic plaques and upregulated by oxidized LDL. Circulation 104:3103–3108
28. Kume S, Uzu T, Araki S et al (2007) Role of altered renal lipid metabolism in the development of renal injury induced by a high-fat diet. J Am Soc Nephrol 18:2715–2723
29. Okamura DM, Pennathur S, Pasichnyk K et al (2009) CD36 regulates oxidative stress and inflammation in hypercholesterolemic CKD. J Am Soc Nephrol 20:495–505
30. Jiang T, Wang Z, Proctor G et al (2005) Diet-induced obesity in C57BL/6J mice causes increased renal lipid accumulation and glomerulosclerosis via a sterol regulatory element-binding protein-1c-dependent pathway. J Biol Chem 280:32317–32325
31. Croce K, Gao H, Wang Y et al (2009) Myeloid-related protein-8/14 is critical for the biological response to vascular injury. Circulation 120:427–436
32. Loser K, Vogl T, Voskort M et al (2010) The Toll-like receptor 4 ligands Mrp8 and Mrp14 are crucial in the development of autoreactive CD8+ T cells. Nat Med 16:713–717
33. Burkhardt K, Schwarz S, Pan C et al (2009) Myeloid-related protein 8/14 complex describes microcirculatory alterations in patients with type 2 diabetes and nephropathy. Cardiovasc Diabetol 8:10
34. Bouma G, Lam-Tse WK, Wierenga-Wolf AF, Drexhage HA, Versnel MA (2004) Increased serum levels of MRP-8/14 in type 1 diabetes induce an increased expression of CD11b and an enhanced adhesion of circulating monocytes to fibronectin. Diabetes 53:1979–1986
35. Yamamoto Y, Kato I, Doi T et al (2001) Development and prevention of advanced diabetic nephropathy in RAGE-overexpressing mice. J Clin Invest 108:261–268
36. Furuta T, Saito T, Ootaka T et al (1993) The role of macrophages in diabetic glomerulosclerosis. Am J Kidney Dis 21:480–485
37. Sassy-Prigent C, Heudes D, Mandet C et al (2000) Early glomerular macrophage recruitment in streptozotocin-induced diabetic rats. Diabetes 49:466–475
38. Usui HK, Shikata K, Sasaki M et al (2007) Macrophage scavenger receptor-a-deficient mice are resistant against diabetic nephropathy through amelioration of microinflammation. Diabetes 56:363–372
39. Chow FY, Nikolic-Paterson DJ, Ozols E, Atkins RC, Rollin BJ, Tesch GH (2006) Monocyte chemoattractant protein-1 promotes the development of diabetic renal injury in streptozotocin-treated mice. Kidney Int 69:73–80
40. Chow FY, Nikolic-Paterson DJ, Ma FY, Ozols E, Rollins BJ, Tesch GH (2007) Monocyte chemoattractant protein-1-induced tissue inflammation is critical for the development of renal injury but not type 2 diabetes in obese db/db mice. Diabetologia 50:471–480
41. Kanamori H, Matsubara T, Mima A et al (2007) Inhibition of MCP-1/CCR2 pathway ameliorates the development of diabetic nephropathy. Biochem Biophys Res Commun 360:772–777
42. Sayyed SG, Ryu M, Kulkarni OP et al (2011) An orally active chemokine receptor CCR2 antagonist prevents glomerulosclerosis and renal failure in type 2 diabetes. Kidney Int 80:68–78
43. Yokoi H, Mukoyama M, Sugawara A et al (2002) Role of connective tissue growth factor in fibronectin expression and tubulointerstitial fibrosis. Am J Physiol Renal Physiol 282:F933–942
44. Takano Y, Yamauchi K, Hayakawa K et al (2007) Transcriptional suppression of nephrin in podocytes by macrophages: roles of inflammatory cytokines and involvement of the PI3K/Akt pathway. FEBS Lett 581:421–426
45. Lee EY, Chung CH, Khoury CC et al (2009) The monocyte chemoattractant protein-1/CCR2 loop, inducible by TGF-beta, increases podocyte motility and albumin permeability. Am J Physiol Renal Physiol 297:F85–94
46. Kwoh C, Shannon MB, Miner JH, Shaw A (2006) Pathogenesis of nonimmune glomerulopathies. Annu Rev Pathol 1:349–374
47. Kagan JC, Su T, Horng T, Chow A, Akira S, Medzhitov R (2008) TRAM couples endocytosis of Toll-like receptor 4 to the induction of interferon-beta. Nat Immunol 9:361–368

THE JOURNAL OF BIOLOGICAL CHEMISTRY VOL. 287, NO. 48, pp. 40441–40447, November 23, 2012

Leptin Activates Hepatic 5′-AMP-activated Protein Kinase through Sympathetic Nervous System and α1-Adrenergic Receptor

*A POTENTIAL MECHANISM FOR IMPROVEMENT OF FATTY LIVER IN LIPODYSTROPHY BY LEPTIN**

Received for publication, June 16, 2012, and in revised form, September 24, 2012 Published, JBC Papers in Press, September 28, 2012, DOI 10.1074/jbc.M112.384545

Licht Miyamoto[‡1], Ken Ebihara[‡§2], Toru Kusakabe[‡], Daisuke Aotani[‡], Sachiko Yamamoto-Kataoka[‡], Takeru Sakai[‡], Megumi Aizawa-Abe[‡§], Yuji Yamamoto[‡], Junji Fujikura[‡], Tatsuya Hayashi[¶], Kiminori Hosoda[‡§‖], and Kazuwa Nakao[‡§]

From the [‡]Department of Medicine and Clinical Science, Kyoto University Graduate School of Medicine and the [§]Translational Research Center, Kyoto University Hospital, 54 Shogoin Kawahara-cho, Sakyo-ku, Kyoto 606-8507, the [¶]Kyoto University Graduate School of Human and Environmental Studies, Yoshida-Nihonmatsu-cho, Sakyo-ku, Kyoto 606-8501, and the [‖]Department of Human Health Science, Kyoto University Graduate School of Medicine, 54 Shogoin Kawahara-cho, Sakyo-ku, Kyoto 606-8507, Japan

Background: AMPK activation promotes glucose and lipid metabolism.
Results: Hepatic AMPK activities were decreased in fatty liver from lipodystrophic mice, and leptin activated the hepatic AMPK via the α-adrenergic effect.
Conclusion: Leptin improved the fatty liver possibly by activating hepatic AMPK through the central and sympathetic nervous systems.
Significance: Hepatic AMPK plays significant roles in the pathophysiology of lipodystrophy and metabolic action of leptin.

Leptin is an adipocyte-derived hormone that regulates energy homeostasis. Leptin treatment strikingly ameliorates metabolic disorders of lipodystrophy, which exhibits ectopic fat accumulation and severe insulin-resistant diabetes due to a paucity of adipose tissue. Although leptin is shown to activate 5′-AMP-activated protein kinase (AMPK) in the skeletal muscle, the effect of leptin in the liver is still unclear. We investigated the effect of leptin on hepatic AMPK and its pathophysiological relevance in A-ZIP/F-1 mice, a model of generalized lipodystrophy. Here, we demonstrated that leptin activates hepatic AMPK through the central nervous system and α-adrenergic sympathetic nerves. AMPK activities were decreased in the fatty liver of A-ZIP/F-1 mice, and leptin administration increased AMPK activities in the liver as well as in skeletal muscle with significant reduction in triglyceride content. Activation of hepatic AMPK with A769662 also led to a decrease in hepatic triglyceride content and blood glucose levels in A-ZIP/F-1 mice. These results indicate that the down-regulation of hepatic AMPK activities plays a pathophysiological role in the metabolic disturbances of lipodystrophy, and the hepatic AMPK activation is involved in the therapeutic effects of leptin.

Leptin is an adipocyte-derived hormone that regulates energy homeostasis mainly through the hypothalamus (1, 2). In addition to food intake and energy expenditure, leptin regulates glucose and lipid metabolism. Indeed, the usefulness of leptin treatment in various types of diabetes, including type 1, type 2, and lipoatrophic diabetes, has been demonstrated in rodent models (3–8). The clinical application of leptin treatment has already begun (9–12), especially in lipoatrophic diabetes that develops with lipodystrophy.

Lipodystrophy is a disease characterized by a paucity of adipose tissue that leads to leptin deficiency. Patients with lipodystrophy generally suffer severe insulin-resistant diabetes. Although the molecular mechanism by which insulin resistance develops in lipodystrophy is not fully understood, ectopic fat accumulation in insulin target tissues such as skeletal muscle and liver is thought to be one of the major causes for insulin resistance. The pathological condition in which ectopically accumulated fat exerts adverse effects against the cellular function is referred to as "lipotoxicity" (13). The amount of fat accumulated in tissues is known to correlate with the severity of insulin resistance (14). Lipoatrophic patients frequently develop severe fatty liver and excess fat accumulation in the skeletal muscle (15).

We and others have demonstrated that leptin effectively improves insulin sensitivity accompanied by dramatic reduction of fat content in the liver and skeletal muscle in patients

* This work was supported in part by research grants from the Ministry of Education, Culture, Sports, Science and Technology of Japan, the Ministry of Health, Labor and Welfare of Japan, The Takeda Medical Research Foundation, The Japan Foundation of Applied Enzymology, Eli Lilly and Co., and The Nakatomi Foundation.
[1] Present address: Dept. of Medical Pharmacology, Institute of Health Biosciences, University of Tokushima Graduate School, 1-78-1 Shou-machi, Tokushima-shi, Tokushima 770-8505, Japan.
[2] To whom correspondence should be addressed: 54 Shogoin Kawahara-cho, Sakyo-ku, Kyoto 606-8507, Japan. Tel.: 81-757513173; Fax: 81-757719452; E-mail: kebihara@kuhp.kyoto-u.ac.jp.

with lipodystrophy (3, 9–12). Using rodent models, it was demonstrated that leptin activates AMPK[3] in the skeletal muscle through both central and direct pathways (16). AMPK is a heterotrimeric enzyme that is conserved from yeast to humans and functions as a "fuel gauge" to monitor the status of cellular energy. AMPK potently stimulates fatty acid oxidation by inhibiting the activity of acetyl-CoA carboxylase (17). Thus, AMPK activation by leptin is a plausible mechanism by which leptin reduces ectopic fat in the skeletal muscle.

In addition to the skeletal muscle, recent studies have shown the physiological significance of AMPK in the liver (18–20). However, the effect of leptin on hepatic AMPK activity remains to be determined. The role of AMPK in the pathogenesis of metabolic abnormalities in lipodystrophy also remains unclear. In this study, we investigated the effect of leptin on hepatic AMPK activities and the pathophysiological role of AMPK in A-ZIP/F-1 mice, a well established mouse model of generalized lipodystrophy (21).

EXPERIMENTAL PROCEDURES

Materials and Animals—All reagents were analytic grade and obtained from Sigma unless otherwise stated. C57BL/6J mice and Wistar rats were purchased from Japan SLC, Inc. The F1 mice analyzed in Fig. 4 were obtained by crossing male A-ZIP/F-1 mice on the FVB/N background with female leptin transgenic mice on the C57BL/6J background (3, 22). A-ZIP/F-1 and the F1 mice were studied with appropriate littermate controls. Mice and rats were housed in an animal facility maintained at 20 °C with a 12:12-h light/dark cycle, allowed free access to water and standard rodent chow, and were randomly assigned to experimental groups. The mice were analyzed at the age of 9–10 weeks (C57BL/6J) or 15 weeks (A-ZIP/F-1, F1). Kyoto University Graduate School of Medicine Committee on Animal Research approved all experimental procedures.

Drug Administration—For continuous treatment, leptin was administered for 6 days using a subcutaneously implanted osmotic pump (Durect) at the dose of 0.65 mg/kg/day. For single intraperitoneal and intracerebroventricular (i.c.v.) injection, the dose of leptin was 1 mg/kg and 1 μg/mouse, respectively. Prazosin (2.5 mg/kg/day) or propranolol (1 mg/kg/day) was continuously co-administered with leptin for 6 days using an independently implanted osmotic pump. A769662 was administered once daily by intraperitoneal injection at the dose of 30 mg/kg/day for 4 days.

Primary Hepatocyte—Hepatocytes were isolated from male Wistar rats (100–150 g) by a two-step collagenase perfusion. The portal vein was cannulated under chloral hydrate anesthesia, and the liver was perfused with hepatocyte liver perfusion medium and digest medium (Invitrogen). After perfusion, hepatocytes were purified by filtration (100-μm mesh) and centrifuged (100 × *g*, 1 min, four times) and seeded onto 6-well culture plates coated with type I collagen (Iwaki) (1×10^6 cells/well). Cells were cultured in DMEM containing 10% FBS, 100 nM insulin, 100 nM dexamethasone, 30 mg/liter kanamycin, and 5 units/ml aprotinin for 12 h, and the medium were replaced with DMEM containing 10% FBS, 1 nM insulin, 1 nM dexamethasone, 30 mg/liter kanamycin, and 5 units/ml aprotinin for 6 h prior to stimulation. The cells were stimulated by 100 ng/ml leptin, 1 mM 5-aminoimidazole-4-carboxamide 1-β-D-ribofuranoside or 0.5 mM 2,4-dinitrophenol for the indicated times.

Hepatic Vagotomy—Hepatic vagotomy was performed as described previously (23, 24) with modifications. Briefly, a hepatic branch of the ventral subdiaphragmatic vagal trunk was cleft using micro scissors under ether anesthesia, and the abdominal muscle wall and skin incision was closed with silk sutures. Drugs were introduced 1 week after the surgery. Accomplishment of the amputation was visually confirmed when sampling.

Chemical Sympathectomy—C57BL/6J mice were chemically sympathectomized by continuous infusion of guanethidine (30 mg/kg/day) for 6 days as described above.

Tissue Sampling and Biochemical Analysis—Tissues were rapidly isolated and frozen in liquid nitrogen by freeze-clamping (25) under chloral hydrate anesthesia after starvation for 6 h. Mice had been starved for 4 h previous to and during the study in a single administration study. Blood glucose was determined by reflectance glucometer under *ad libitum* feeding conditions. Plasma leptin was measured by RIA (Linco). Plasma insulin (Morinaga), adiponectin (Linco), and interleukin-6 (R&D Systems) were measured by ELISA. Triglyceride content was determined by E-test kit (Wako) in 2-propanol/heptane extract of the tissues. Homeostasis model assessment insulin resistance (HOMA-IR) was calculated on the assumption that the titer of murine insulin is as much as that of human insulin.

Isoform-specific AMPK Activity—AMPK activities were determined as described previously (26). Briefly, frozen tissues were homogenized in Hepes/Triton-based lysis buffer and then centrifuged. The supernatants were immunoprecipitated with protein A-Sepharose beads and isoform-specific antibodies against AMPK α1 or α2 (Millipore). Kinase activities in the immune complex were determined by the phosphorylation of the SAMS peptide using [γ-^{32}P]ATP.

Western Blotting Analysis—40 μg of protein per each sample was subjected to SDS-PAGE using 4–12% BisTris gel (Bio-Rad). Antibodies were from Cell Signaling Technology or Merck. ECL Plus (GE Healthcare) and LAS-1000 image analyzer (Fuji film) were used for detection and quantification.

Quantitative Analysis of Gene Expressions—Total RNA was prepared using Isogen (Molecular Research Center). mRNA levels were quantified by real time PCR with the Taqman method (ABI Prism 7300). Primer sets and probes were as follows: 18 S, CGCGCAAATTACCCACTCCCGA, CGGCTACCACATCCAAGGA, and CCAATTACAGGGCCTCGAAA; AMPKα1, TGCAAAGATAGCCGACTTTGGTCTTTCA, GAACGTCCTGCTTGATGCACACAT, and TGGGTGAGCCACAGCTTGTTCTTA; and AMPKα2, TGATTCCAGCACAGCTGAGAACCACT, AAGCATCGATGATGAGGTGGTGGA, and ACAAAGTGCTGCCAGTCAAAGAGC (probe, forward, and reverse, respectively) Relative amounts of mRNAs were normalized with the ribosomal 18 S RNA.

[3] The abbreviations used are: AMPK, 5′-AMP-activated protein kinase; A-ZIP, A-ZIP/F-1 mice; LepTg, transgenic mice overexpressing leptin; BisTris, 2-[bis(2-hydroxyethyl)amino]-2-(hydroxymethyl)propane-1,3-diol; HOMA-IR, homeostasis model assessment insulin resistance; i.c.v., intracerebroventricular.

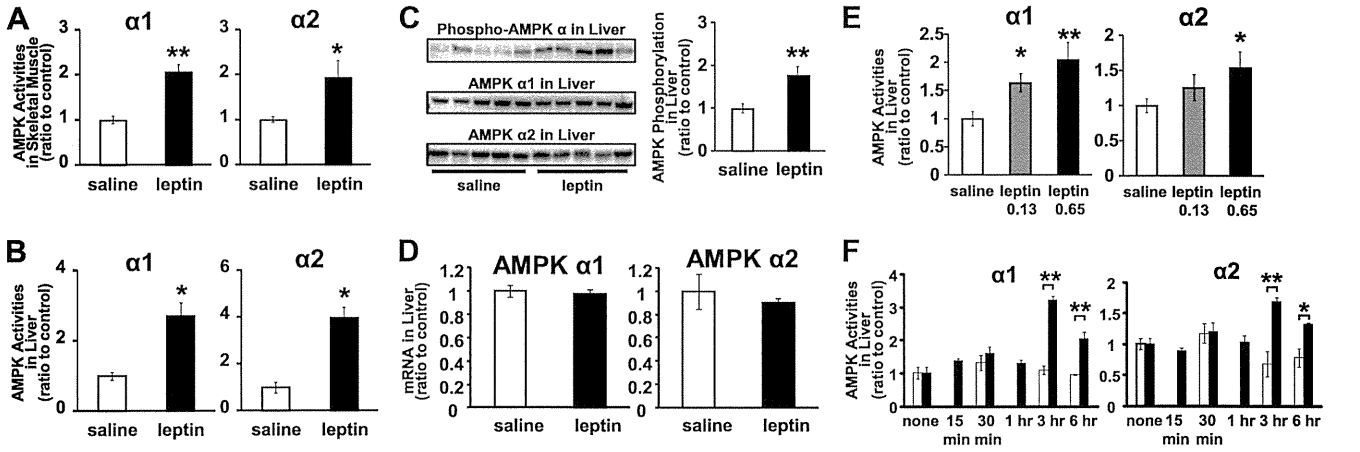

FIGURE 1. **AMPK activation in skeletal muscle and liver by leptin administration.** Isoform-specific AMPK activities in gastrocnemius muscle (*A*) and liver (*B*) from C57BL/6J mice after continuous saline or leptin administration are shown. Western blot analyses for phospho-AMPKα, AMPK α1 and α2 (*C*), and AMPK α1 and α2 mRNA levels normalized to 18 S ribosomal RNA (*D*) in liver are shown. AMPK activities in liver after 0.13 and 0.65 mg/kg/day continuous leptin infusion (*E*) are shown. AMPK activities in liver 15 min to 6 h after single intraperitoneal injection of saline or leptin (*F*) are shown. Data are shown as ratios to saline or quiescent control (mean ± S.E.). □, saline; ■, leptin. $n = 4-6$. *, $p < 0.05$; **, $p < 0.01$ *versus* saline.

Statistical Analyses—Two groups were compared by Student's *t* test. Comparisons between multiple groups were evaluated by analysis of variance. $p < 0.05$ was considered statistically significant.

RESULTS

Effect of Leptin Treatment on AMPK α1 and α2 Activities in Skeletal Muscle and Liver—The isoform-specific AMPK activities in skeletal muscles and liver were determined in leptin- and saline-treated mice. Both AMPK α1 and α2 activities in skeletal muscle were increased 2-fold in leptin-treated mice compared with saline-treated mice (Fig. 1*A*). AMPK α1 and α2 activities in the liver were also increased 2.5- and 3.5-fold, respectively (Fig. 1*B*). The phosphorylation of AMPK α was also increased in leptin-treated mice compared with saline-treated mice (Fig. 1*C*). Meanwhile, protein or mRNA expressions of AMPK α1 and α2 in the liver were not significantly different between leptin- and saline-treated mice (Fig. 1, *C* and *D*). Therefore, the increase of AMPK activities in the liver from leptin-treated mice was not due to the increase in their expression levels.

When leptin was administered continuously, the activation of AMPK in the liver was dose-dependent (Fig. 1*E*). After intraperitoneal single leptin injection, the activation of both AMPK α1 and α2 was detected from 3 h while no activation was observed within 1 h (Fig. 1*F*).

Mechanism of Hepatic AMPK Activation by Leptin—To clarify whether leptin acts directly on hepatocytes, we examined AMPK activities in isolated primary rat hepatocytes with or without leptin (Fig. 2*A*). The addition of leptin into the culture medium increased neither AMPK α1 nor α2 activities. Next, we examined the effect of leptin i.c.v. injection on AMPK activities in the liver (Fig. 2*B*). The activation of both AMPK α1 and α2 was detected 3 h after leptin injection at the dose that did not cause any effect when administered peripherally. These results indicate that leptin activates AMPK in the liver mainly through the CNS.

Therefore, we examined the involvement of autonomic nerves in the effect of leptin on AMPK activation in the liver. Hepatic vagotomy did not show any effect on AMPK activation by leptin in the liver (Fig. 2*C*). In contrast, chemical sympathectomy by guanethidine treatment completely inhibited the activation of both AMPK α1 and α2 by leptin in the liver (Fig. 2*D*). We further investigated the involvement of the subtype-specific sympathetic nervous system. Administration of propranolol, a β-antagonist, did not suppress AMPK activation in the liver, whereas prazosin, an α1-antagonist, completely inhibited the activation of both AMPK α1 and α2 by leptin in the liver (Fig. 2, *E* and *F*).

AMPK α1 and α2 Activities in Skeletal Muscle and Liver from A-ZIP/F-1 Mice—To explore the pathophysiological role of AMPK in lipodystrophy, we examined AMPK α1 and α2 activities in skeletal muscle and liver from A-ZIP/F-1 (A-ZIP) mice. Characteristics of A-ZIP mice used in this study are shown in Table 1. Consistent with previous studies (21), A-ZIP mice showed hyperglycemia and hyperinsulinemia, suggesting insulin resistance, and also showed increased liver weight, suggesting fatty liver. Plasma leptin and adiponectin levels were markedly decreased, but the plasma interleukin-6 level was not significantly different from that in WT mice. In these A-ZIP mice, both AMPK α1 and α2 activities in the liver were apparently decreased compared with WT mice, although those in the skeletal muscle were not significantly different from WT mice (Fig. 3, *A* and *B*). AMPK α1 and α2 mRNA expressions in the skeletal muscle were not significantly different in A-ZIP mice, and those in the liver were rather increased compared with WT mice (Fig. 3, *C* and *D*). Therefore, the decrease in AMPK activities in the liver from A-ZIP mice was not due to the change in their mRNA expressions. However, leptin treatment effectively increased AMPK α1 and α2 activities in the liver as well as in the skeletal muscle from A-ZIP mice (Fig. 3, *E* and *F*).

Effect of Transgenic Overexpression of Leptin on AMPK α1 and α2 Activities in Skeletal Muscle and Liver from A-ZIP/F-1 Mice—To explore the chronic effect of leptin, we crossed transgenic mice overexpressing leptin (LepTg) and A-ZIP mice, producing mice of four genotypes as follows: WT, LepTg, A-ZIP, and A-ZIP/LepTg. AMPK α1 and α2 activities in both the skel-

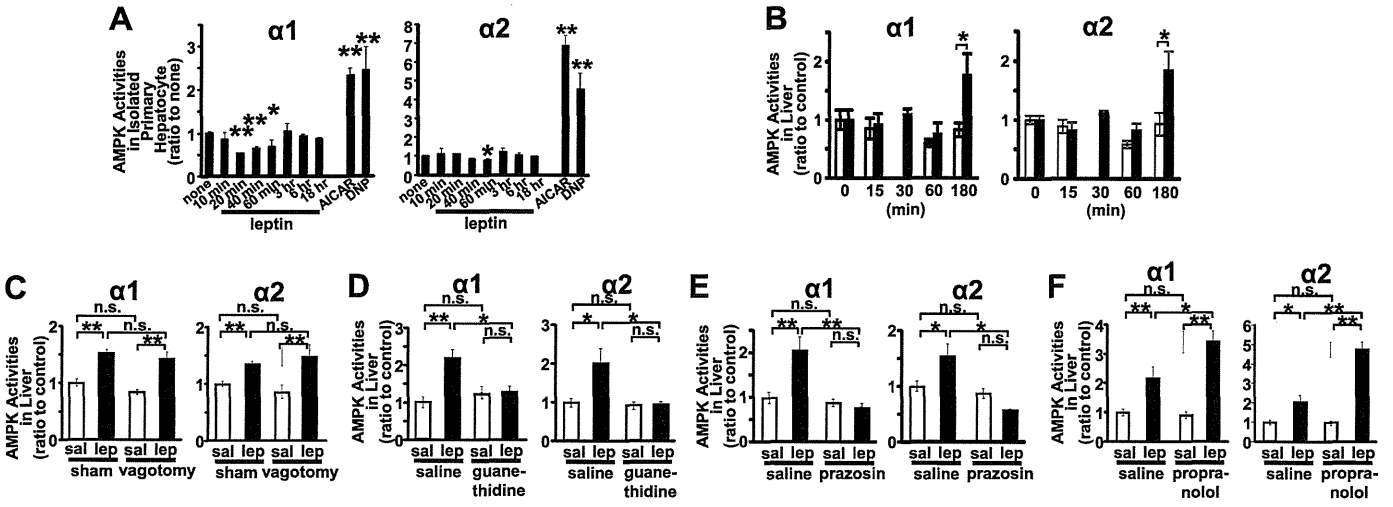

FIGURE 2. **Mechanism of hepatic AMPK activation by leptin administration.** AMPK activities in isolated rat primary hepatocytes 10 min to 18 h after stimulation by leptin, 5-aminoimidazole-4-carboxamide 1-β-D-ribofuranoside (*AICAR*) (40 min), or 2,4-dinitrophenol (*DNP*) (15 min) (*A*) are shown. AMPK activities in liver 15 min to 3 h after i.c.v. administration of saline (*sal*) or leptin (*lep*) (*B*). The effects of hepatic vagotomy (*C*), chemical sympathectomy (*D*), co-administration of antagonists against α1-adrenoreceptors (*E*) or β-adrenoreceptors (*F*) on hepatic AMPK activation by leptin are shown. Data are shown as ratios to saline or quiescent control (mean ± S.E.). $n = 4–6$ (*A*, and *C–E*); $n = 3–6$ (*B*). *, $p < 0.05$; **, $p < 0.01$ *versus* control. *n.s.*, not significant.

TABLE 1

Characteristics of A-ZIP/F-1 mice used in this study

Values are as follows: $n = 8–11$ (glucose); $n = 3–5$ (leptin); $n = 5–7$ (other adipocytokines).

	WT	A-ZIP/F-1 mice
Body weight	30.7 ± 0.8 g	32.5 ± 0.4 g
Glucose	167 ± 5.8 mg/dl	331 ± 39 mg/dl[a]
Insulin	0.24 ± 0.0 ng/ml	0.46 ± 0.1 ng/ml[b]
Leptin	6.15 ± 1.3 ng/ml	1.25 ± 0.5 ng/ml[b]
Adiponectin	6.27 ± 0.4 μg/ml	1.46 ± 0.5 μg/ml[a]
Interleukin-6	5.3 ± 0.8 pg/ml	6.5 ± 1.0 pg/ml
Liver weight	1.19 ± 0.0 g	1.98 ± 0.2 g[a]

[a] $p < 0.01$ *versus* WT. Data are expressed as means ±S.E.
[b] $p < 0.05$ *versus* WT. Data are expressed as means ±S.E.

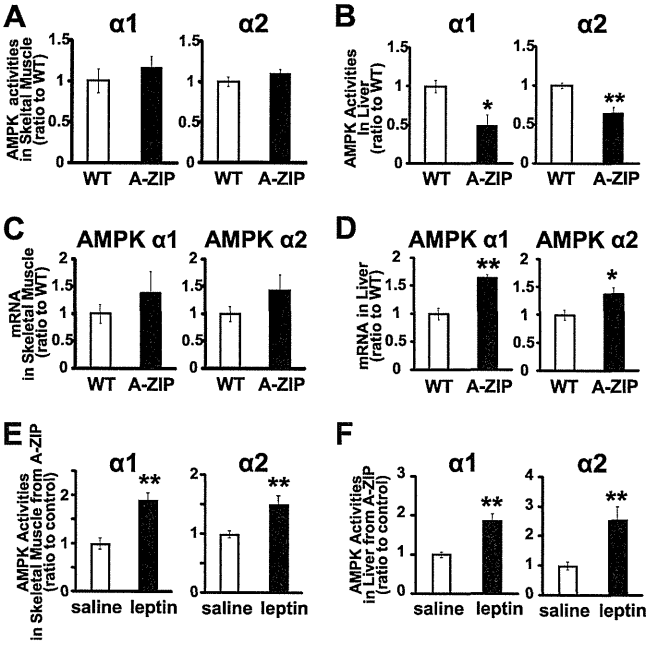

FIGURE 3. **AMPK activities and mRNA expressions in a mouse model of lipoatrophic diabetes.** α1- and α2-isoform-specific AMPK activities in the soleus muscle (*A*) and liver (*B*) are shown. AMPK α1 and α2 mRNA levels in the soleus muscle (*C*) and liver (*D*) normalized to 18 S ribosomal RNA are shown. AMPK activities in gastrocnemius muscle (*E*) and liver (*F*) from A-ZIP/F-1 mice after continuous leptin administration are shown. Data are shown as ratios to WT or saline control (mean ± S.E.). □, WT; ■, A-ZIP/F-1. $n = 4–5$. (*A–D*). □, saline; ■, leptin. $n = 9–10$ (*E* and *F*). *, $p < 0.05$; **, $p < 0.01$ *versus* control.

etal muscle and liver were markedly increased in LepTg mice (Fig. 4, *A* and *B*). At this time, triglyceride contents in skeletal muscle and liver in LepTg mice were reduced to more than half of those in WT mice (Fig. 4, *C* and *D*). AMPK activities were unchanged in the skeletal muscle but were apparently decreased in the liver from A-ZIP mice when compared with WT mice (Fig. 4, *A* and *B*). As to triglyceride contents, the apparent increment was observed in both the skeletal muscle and liver in A-ZIP mice (Fig. 4, *C* and *D*). However, AMPK activities were increased, and triglyceride content was decreased in A-ZIP/LepTg mice as well as in LepTg mice in both the skeletal muscle and liver (Fig. 4, *A–D*). In accordance with our previous report, blood glucose and plasma insulin levels were lower in LepTg mice than in WT mice, and severe hyperglycemia and hyperinsulinemia in A-ZIP mice were strikingly ameliorated by transgenic overexpression of leptin (Fig. 4, *E* and *F*) (3).

Effect of AMPK Activator, A769662, on AMPK Activities and Triglyceride Content in Skeletal Muscle and Liver from A-ZIP/F-1 Mice—After intraperitoneal single injection of A769662, an AMPK-specific activator, the activity of AMPK α1 was increased but that of α2 was not significantly increased in the skeletal muscle (Fig. 5*A*). The activity of both AMPK α1 and α2 was clearly increased in the liver (Fig. 5*B*). Although repetitive injection of A769662 for 4 days did not significantly reduce triglyceride content in the skeletal muscle, it effectively reduced triglyceride content to one-third of that in saline-treated mice in the liver (Fig. 5, *C* and *D*). At this time, the blood glucose level was significantly decreased, and HOMA-IR, an index of insulin resistance, tended to be decreased although plasma insulin level was not significantly decreased (Fig. 5, *E–G*). Food intake and body weight were not affected by A769662 (Fig. 5, *H* and *I*).